

# Geochemistry of Middle Oligocene–Pliocene sandstones from the Nanpu Sag, Bohai Bay Basin (Eastern China): Implications for provenance, weathering, and tectonic setting

SHILIN LIU,<sup>1,2</sup> GE LIN,<sup>1\*</sup> YUNHUA LIU,<sup>3</sup> YE ZHOU,<sup>1,2</sup> FAXIONG GONG<sup>1,2</sup> and YI YAN<sup>1</sup>

<sup>1</sup>Key Laboratory of Marginal Sea Geology, Guangzhou Institute of Geochemistry, Chinese Academy of Sciences, Guangzhou 510640, China

<sup>2</sup>Graduate School, Chinese Academy of Sciences, Beijing 100039, China

<sup>3</sup>Research Institute of Jidong Oilfield Company, CNPC, Tangshan 063004, China

(Received February 2, 2007; Accepted July 23, 2007)

Petrographic and geochemical compositions of thirty-seven Middle Oligocene–Pliocene sandstone samples from the Nanpu Sag in Bohai Bay Basin were analyzed to evaluate their provenance, weathering, and tectonic setting. These sandstones comprise mainly arkoses and lithic arenites and a few graywackes, characterized by low to moderate quartz/total feldspar ratios ( $1.31\text{--}6.11$ , average  $2.72 \pm 0.98$ ) and CIA values ( $45.87\text{--}70.13$ ,  $57.49 \pm 5.93$ ). The Middle–Upper Oligocene sandstones have average lower  $\text{SiO}_2$  ( $71.72 \pm 5.16\%$ ), and higher  $\text{Fe}_2\text{O}_3$  ( $3.06 \pm 1.26\%$ ) and  $\text{MgO}$  ( $1.65 \pm 0.39\%$ ), in contrast with the Miocene samples that generally have high  $\text{SiO}_2$  ( $76.46 \pm 4.26\%$ ) and low  $\text{Fe}_2\text{O}_3$  ( $3.04 \pm 1.51\%$ ) and  $\text{MgO}$  ( $0.69 \pm 0.32\%$ ) contents. Following the deposition,  $\text{Fe}_2\text{O}_3$  ( $3.17 \pm 1.00\%$ ) and  $\text{MgO}$  ( $1.07 \pm 0.38\%$ ) contents increased again in the Pliocene samples. Such a compositional variation trend is interpreted as a change of tectonic activity in the sag from Middle Oligocene to Pliocene, i.e., stronger in the Middle Oligocene, weaker in the Miocene and to stronger again in the Pliocene. Qt–F–L plot, trace element provenance discrimination diagrams (e.g.,  $\text{Eu}/\text{Eu}^*$ ,  $\text{Co}/\text{Th}$ , and  $\text{La}/\text{Sc}$ ), and REE characteristics suggest that the source rocks were mainly derived from felsic igneous rocks, possibly from Mesozoic granitoids and felsic volcanic lavas in the Yanshan Fold Belt. Tectonic discrimination diagrams (e.g.,  $\text{SiO}_2\text{--K}_2\text{O}/\text{Na}_2\text{O}$ ,  $\text{Fe}_2\text{O}_3^* + \text{MgO--TiO}_2$ , and  $\text{Th--Sc--Zr}/10$ ) show that these sandstones were mainly deposited in an active continental margin setting, implying a remobilized intra-continental environment.

Keywords: petrography, geochemistry, provenance, tectonic setting, Nanpu Sag

## INTRODUCTION

Clastic sedimentary rocks contain important information about the composition, tectonic setting and evolution of continental crust, especially when the traditional petrographic techniques are ambiguous. Although their chemical record can be affected by factors such as source rock characteristics, chemical weathering, and sorting processes during transportation, sedimentation and post-depositional diagenesis (McLennan, 1989; Nesbitt and Young, 1996; Nesbitt *et al.*, 1996), some immobile elements such as Y, Sc, Th, Zr, Hf, Cr, Co and rare earth elements (REE) are believed to be useful indicators of geological processes, provenance and tectonic setting (Cullers *et al.*, 1987, 1988; Bhatia and Crook, 1986; Taylor and McLennan, 1985; McLennan *et al.*, 1993). Therefore,

the geochemistry of clastic sediments can be effectively used to understand their tectonic setting and provenance (Bhatia, 1983; Roser and Korsch, 1986, 1988; Condie *et al.*, 1992). On this basis, many recent geochemical studies on sandstones and shales have focused on delineating the provenance and tectonic evolution of sedimentary basins (Armstrong-Altrin *et al.*, 2004; Wanas and Abdel-Maguid, 2006).

The Bohai Bay Basin has attracted the attention of many researchers not only for its abundant petroleum resources, but also for its tectonic evolution. Various viewpoints have been proposed about the origin of the basin, but its dynamic mechanism and tectonic setting are still in dispute (Guo *et al.*, 2005). Most researchers emphasized the extensional model, and believed that Bohai Bay Basin should be an actively rifted basin under the regional extension due to the upwelling of mantle or asthenosphere (Ma *et al.*, 1983; Lu *et al.*, 1997), and the mantle or asthenosphere upwelling had a close relationship with the subduction of the Pacific plate towards the Eurasian plate. Natural seismic image and long-wave geoelectromagnetic

\*Corresponding author (e-mail: gelin@gig.ac.cn)

deep sounding have shown that in eastern China the subducting Pacific plate probably reaches in the upper/lower mantle interface at a depth of 670 km and with a length of over 1000 km (Fukao and Maruyama, 1994; Ichiki *et al.*, 2001). With respect to the NNW-trending underthrusting Pacific plate, the Eurasian plate has an overthrusting trend towards SEE (Guo *et al.*, 2003). This may not only have caused back-arc extension of continental lithosphere as a result of upwelling of mantle materials in eastern China (Xu *et al.*, 2004), but also resulted in roll-back of the subduction zone. Wang, H. *et al.* (2002) pointed out that in the Nanpu Sag the depth of the top of the asthenosphere varied from 66.5 km to 56 km from the Late Oligocene to Pliocene, suggesting that an obvious mantle upwelling existed. Recent seismic imaging (Zheng *et al.*, 2006) further revealed that in the Cenozoic Bohai Bay Basin the crust was significantly thinned, due mainly to reduction in the thickness of the lower crust (including the crust-mantle transition zone), by up to ~12 km. Numerical simulation data also demonstrated the existing of roll-back of the subduction zone (Zhang and Shi, 2003). The subduction and roll-back effect of the Pacific plate would have changed the thermal-dynamic states of East Asia, and resulted in the formation of Cenozoic extensional basins such as the Bohai Bay Basin, and large-scale attenuation of the lithosphere in eastern China, especially within these extensional basins. In contrast, a few believed that the basin was a pull-apart or passive rifted basin where a later strike-slip system was juxtaposed on early extensional structures. It may therefore have formed as a pull-apart basin by dextral displacement along NNE-trending normal faults (Zhao, 1984; Chen and Nabelek, 1988). On the other hand, subduction of the Pacific plate towards the Eurasian plate is generally considered as the reason for the origin of the Bohai Bay Basin (Guo *et al.*, 2005), although Zhang (1988) suggested that its formation was related not only to the subduction, but also to the Eurasian plate spreading and creeping towards the ocean.

Nanpu Sag, a small petroliferous sag, is located in the northern Bohai Bay Basin. Most of previous work on it (e.g., Cong and Zhou, 1998; Wang, H. *et al.*, 2002) has focused on the structural styles and sedimentary filling strata, and has made great contributions to the petroleum exploration in this area, rather than the basin itself. Also little attention has been paid to the study of provenance in this sag, even though this is very important for further hydrocarbon exploration and understanding Cenozoic tectonic evolution of eastern China. In this study, petrographic, major, trace, and rare earth element compositions of sandstones of Middle Oligocene to Pliocene age were analyzed to evaluate their provenance, weathering, and tectonic setting.

## GEOLOGICAL SETTING

The Cenozoic Bohai Bay Basin in the eastern part of the North China Block (NCB) is bounded by the Yanshan Fold Belt in the north, by the Luxi Uplift in the south, by the Taihang Mountain Uplift in the west, and by the Jiaoliao Uplift in the east. The basin consists of several NNE-trending depressions and uplift belts (Figs. 1a and b). As one of many secondary structural units in the basin, the Nanpu Sag is bounded by the Xi'nanzhuang Fault in the northwest, by the Baigezhuang Fault in the northeast, and by the Shaleitian Uplift in the south (Fig. 1c). It covers an area of about 2,000 km<sup>2</sup>, and is approximately 50 km long in the E-W direction and 40 km wide in the N-S direction. It is a Cenozoic complex faulted depression developed on pre-Tertiary basin basement.

The regional metamorphic basement in the Nanpu Sag are composed of Archean and Proterozoic crystalline rocks with the oldest age of  $\geq 3.8$  Ga (Liu *et al.*, 1992). The development of the basin since the Paleozoic can be divided into four stages: (1) During the early Paleozoic marine carbonate platform stage, it belonged to the passive continental margin. Carbonate rocks of neritic platform facies dominate the Cambrian and Ordovician sediments. The Caledonian orogeny resulted in a significant unconformity in the basin from the Middle Ordovician to the Middle Carboniferous. (2) The immediate stage from marine to inland basin occurred during the late Paleozoic through the early Mesozoic. Transgression occurred in the Middle Carboniferous. From the Middle Carboniferous to the Early Permian, a series of littoral coal-bearing sediments were formed. During the late Early Permian to Middle Triassic, continental sedimentation prevailed. The Permian and Early–Middle Triassic consist mainly of fluvial and lacustrine red sandstones and mudstones with small amounts of marine sediments (Yang *et al.*, 1986). (3) At the end of the Middle Triassic, a nearly N-S contraction (Indosinian orogeny, *ca.* 250–220 Ma) deformed the pre-Mesozoic strata into a series of NE-trending folds and fault belts, as well as a series of small basins. The Yanshan Fold Belt began to form in this period. From the Early Jurassic to the Early Cretaceous the Yanshanian orogeny formed complex folds and overthrusts. The Yanshan Fold Belt developed rapidly as a response to this intense tectonic-magmatic activation. Upper Triassic–Cretaceous stratigraphies comprise lacustrine and fluvial clastic rocks with several coal-bearing beds (Hu *et al.*, 1989). (4) In Cenozoic, the evolution of the Nanpu Sag as well as other small sags in the Bohai Bay Basin is best described by a two-stage model with a Paleogene synrift phase (including Eocene rifting episode I and Oligocene rifting episode II) and a Neogene postrift phase (including a Miocene thermal subsidence

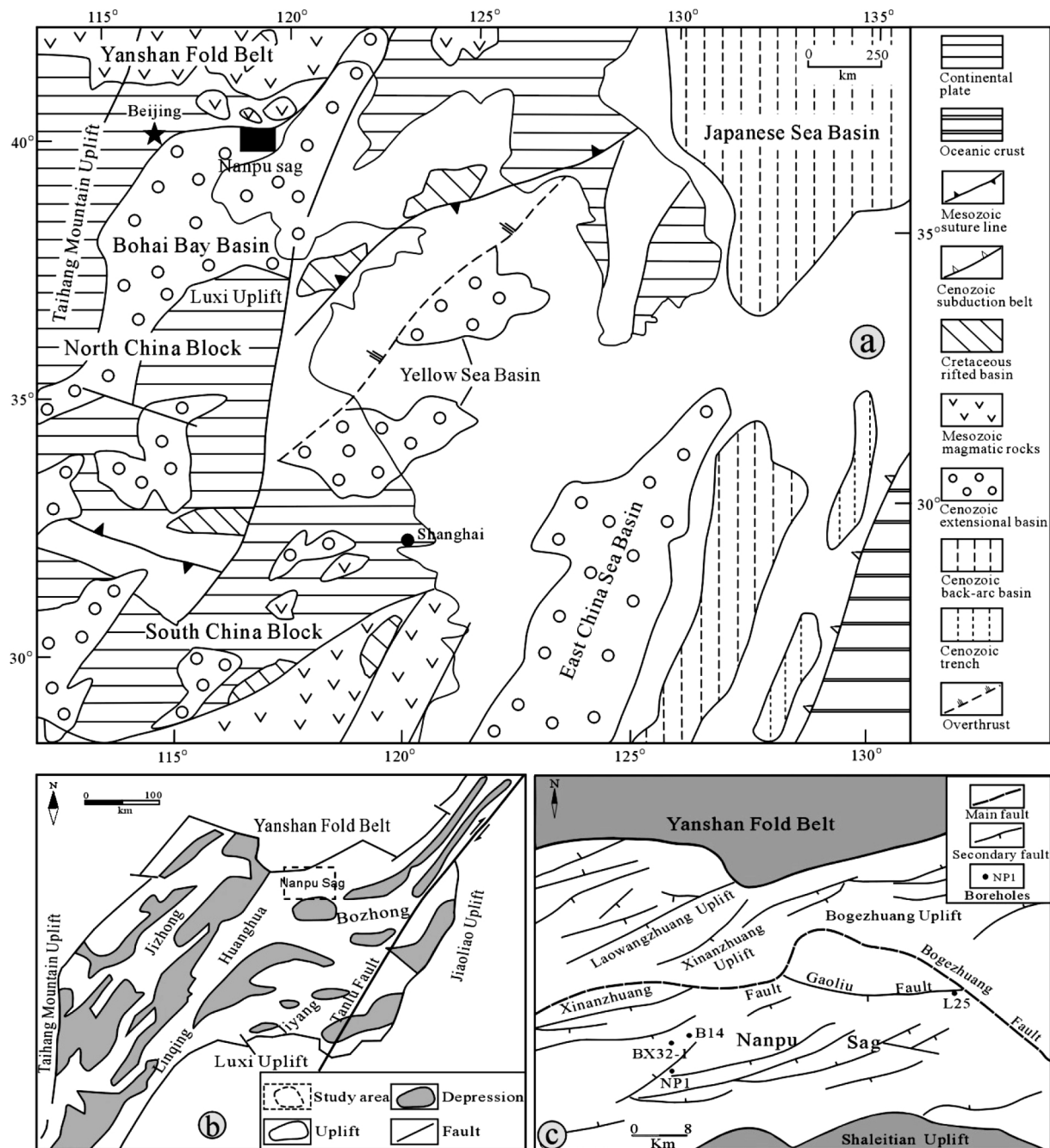


Fig. 1. (a) Location of Nanpu Sag (black rectangle) and Bohai Bay Basin in the North China Block (modified after Ren *et al.*, 2002). Mesozoic–Cenozoic basins in Eastern China and adjacent areas are also shown. (b) General structures in the Bohai Bay Basin. (c) Tectonic sketch map of the Nanpu Sag and the locations of sampled wells in this study (modified after Cong and Zhou, 1998).

period and a Pliocene structural reactivation period) (Ye *et al.*, 1985; Allen *et al.*, 1997; Ren *et al.*, 2002) (Fig. 2).

Tertiary strata of the Nanpu Sag rest unconformably on a variety of older pre-rift strata and are covered conformably or disconformably by Quaternary sediments.

Lithologies are dominated by terrestrial clastic rocks in two main associations: (1) sandstones and organic-rich mudstones formed in lacustrine/fluvial or deltaic environments; (2) purple-red and mottled sandstones and mudstones that formed in alluvial environments. Basal-

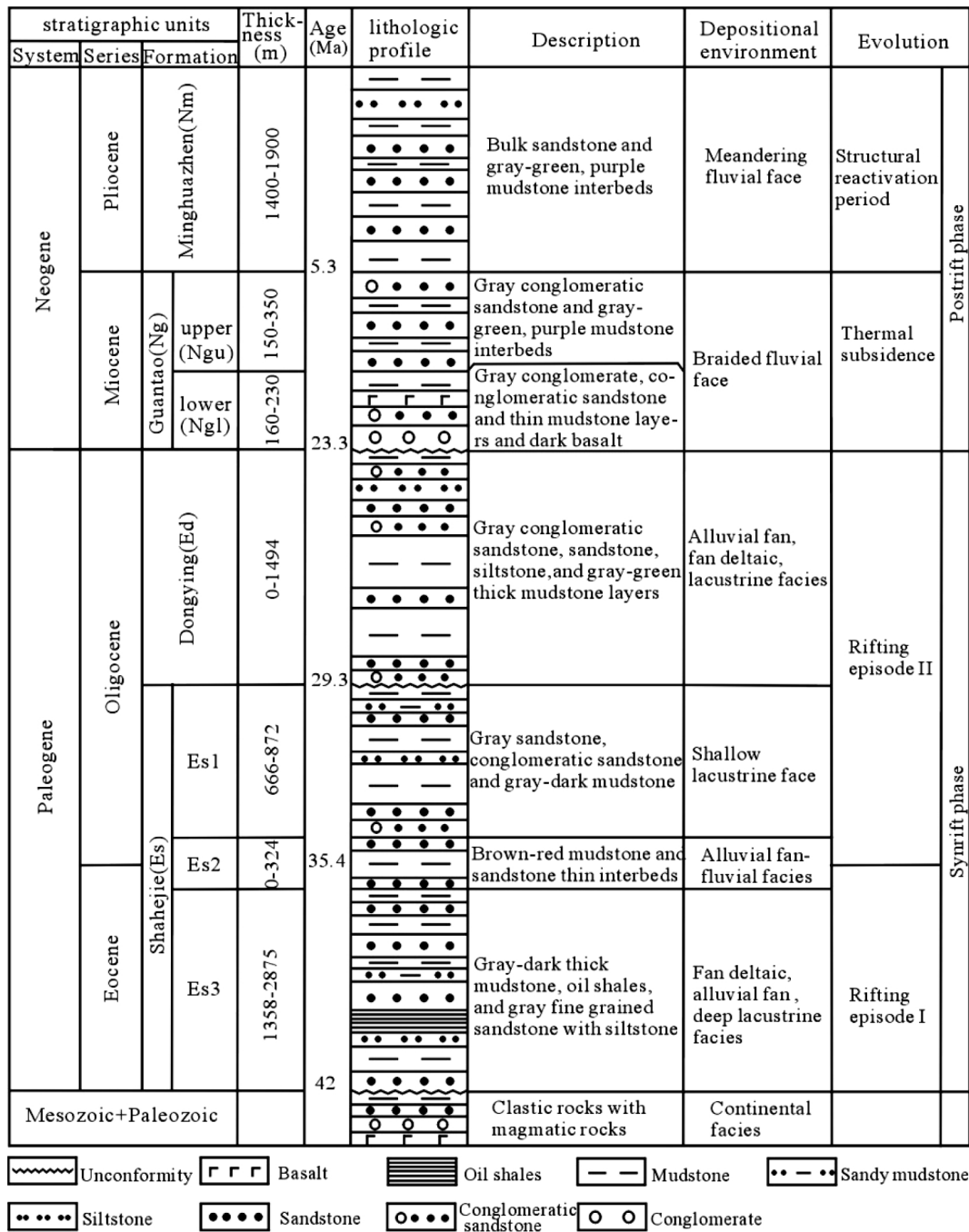


Fig. 2. Tertiary filling sequences and tectonic evolution of the Nanpu Sag (modified after Wang, H. et al., 2002).

tic lavas were extruded locally throughout the Tertiary (Fig. 2). From bottom to top, the Cenozoic Nanpu Sag is filled by Eocene–Early Oligocene Shahejie Formation (abbreviated as Es), Middle–Late Oligocene Dongying Formation (Ed), Miocene Guantao Formation (Ng, including the lower member Ngl and the upper member Ngu), Pliocene Minghuazhen Formation (Nm), and Quaternary sediments (Wang, H. et al., 2002).

## SAMPLING AND METHODS

Due to the oil company's practical needs for hydrocarbon exploration, sampling in the Nanpu Sag was not successive, thus we chose four boreholes to collect samples for this study (Fig. 1c). These boreholes have the same structural-sedimentary features as other boreholes in the sag. Finally thirty-seven fresh moderate-grained

Table 1. The petrography of Middle Oligocene–Pliocene sandstones from the Nanpu Sag in percent

Fm.	Sample	Qm	Qp	P	AF	Lv	Ls	H	M+C	Qn	Qu	Qt	F	L	Lt	Total	Qt:F:L
Nm ( <i>n</i> = 5)																	
	B14-4	44	2	10	8	6	11	1	18	30	14	46	18	17	19	100	57:22:21
	B14-7	41	4	13	12	5	8	2	15	35	6	45	25	13	17	100	54:30:16
	NP1-1 <sup>†</sup>	47	3	8	12	3	3	2	22	38	9	50	20	6	9	100	66:26:8
	NP1-2	42	4	14	11	5	9	2	13	37	5	46	25	14	18	100	54:29:17
	B14-8 <sup>†</sup>	38	4	10	14	4	8	2	20	32	6	42	24	12	16	100	54:31:15
	mean	42	3	11	11	5	8	2	18	34	8	46	22	12	16	100	57:28:15
	s.d.	3	1	2	2	1	3	0	4	3	4	3	3	4	4		5:4:5
Ngu ( <i>n</i> = 19)																	
	B14-10	50	4	9	12	1	9	2	13	40	10	54	21	10	14	100	64:25:11
	B14-12	55	5	7	8	1	8	0	16	48	7	60	15	9	14	100	71:18:11
	B14-13	48	2	7	16	5	12	0	10	41	7	50	23	17	19	100	56:26:18
	B14-15	46	2	7	10	2	11	2	20	40	6	48	17	13	15	100	62:22:16
	B14-16	49	4	6	7	2	12	2	18	39	10	53	13	14	18	100	66:16:18
	B14-17	50	5	6	9	3	7	1	19	40	10	55	15	10	15	100	69:19:12
	L25-8	45	2	8	17	2	8	2	16	40	5	47	25	10	12	100	57:30:13
	L25-9	46	1	12	13	2	7	1	18	40	6	47	25	9	10	100	58:31:11
	NP1-5	44	4	12	11	4	7	1	17	31	13	48	23	11	15	100	59:28:13
	B32X1-26	48	3	8	16	1	4	1	19	39	9	51	24	5	8	100	64:30:6
	B32X1-21	52	4	6	15	0	4	2	17	45	7	56	21	4	8	100	69:26:5
	B32X1-14	54	6	8	12	1	4	1	14	43	11	60	20	5	11	100	71:23:6
	B32X1-13 <sup>†</sup>	34	3	7	13	2	19	1	21	25	9	37	20	21	24	100	47:26:27
	B32X1-12	38	4	8	17	9	4	2	18	29	9	42	25	13	17	100	53:31:16
	B32X1-11 <sup>†</sup>	43	2	8	9	3	12	2	21	35	8	45	17	15	17	100	58:22:20
	B32X1-10	51	6	8	5	3	6	2	19	43	8	57	13	9	15	100	72:16:12
	B32X1-9	44	2	6	11	2	11	3	21	36	8	46	17	13	15	100	61:22:17
	B32X1-6	46	3	7	10	4	9	1	20	40	6	49	17	13	16	100	62:22:16
	B32X1-5	44	6	6	12	3	6	2	21	38	6	50	18	9	15	100	65:23:12
	mean	47	4	8	12	3	8	1	18	39	8	50	19	11	15	100	63:24:13
	s.d.	5	2	2	3	2	4	1	3	5	2	6	4	4	4		7:5:5
Ngl ( <i>n</i> = 9)																	
	L25-10	50	7	4	7	2	8	2	20	45	5	57	11	10	17	100	73:14:13
	L25-11	48	2	5	10	4	7	1	23	36	12	50	15	11	13	100	66:20:14
	L25-12	50	3	6	12	1	4	2	22	40	10	53	18	5	8	100	70:24:6
	B32X1-4	50	3	8	14	1	4	2	18	42	8	53	22	5	8	100	66:28:6
	B32X1-3	49	3	4	9	1	12	1	21	41	8	52	13	13	16	100	67:17:16
	B32X1-2	52	3	6	11	0	6	2	20	43	9	55	17	6	9	100	71:22:7
	B32X1-1	49	4	8	12	2	15	1	9	40	9	53	20	17	21	100	58:22:20
	NP1-4	52	3	5	11	0	9	2	18	41	11	55	16	9	12	100	69:20:11
	NP1-6	49	5	7	8	2	7	2	20	39	10	54	15	9	14	100	69:19:12
	mean	50	4	6	10	1	8	2	19	41	9	54	16	9	13	100	68:20:12
	s.d.	1	2	2	2	1	4	1	4	3	2	2	3	4	4		5:4:5
Ed ( <i>n</i> = 4)																	
	NP1-8	36	4	8	18	2	10	2	20	32	4	40	26	12	16	100	51:33:16
	NP1-9	37	5	6	14	4	10	3	21	31	6	42	20	14	19	100	55:26:19
	NP1-10	32	3	8	13	5	14	2	23	28	4	35	21	19	22	100	47:58:25
	NP1-11	29	5	10	17	5	10	2	22	25	4	34	27	15	20	100	45:36:19
	mean	34	4	8	16	4	11	2	22	29	5	38	24	15	19	100	51:31:18
	s.d.	4	1	2	2	1	2	1	1	3	1	4	4	3	3		5:5:5

Nm = the Pliocene Minghuazhen Formation, Ngu = the upper member of the Miocene Guantao Formation, Ngl = the lower member of the Miocene Guantao Formation, Ed = the Middle-late Oligocene Dongying Formation. Qm: monocrystalline quartz, Qp: polycrystalline quartz, Qn: non-undulose quartz, Qu: undulose quartz, P: plagioclase, AF: alkali feldspar (i.e., orthoclase, microcline), Lv: lithic volcanic clastics, Ls: lithic sedimentary clasts, H: heavy minerals, M + C: matrix + cement, Qt = Qm + Qp, Qm = Qn + Qu, F = P + AF, L = Lv + Ls, Lt = L + Qp, Qm–Lt are listed in percent, s.d. represents the standard deviation, Total =  $\sum(Qm-M + C)$ .

<sup>†</sup>Shows greywacke.

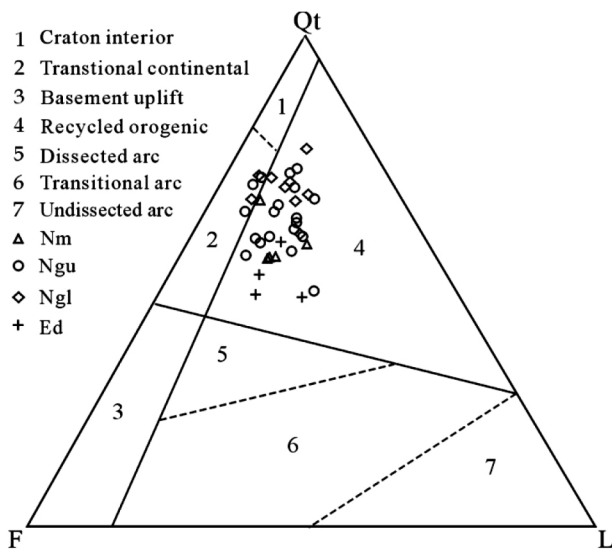


Fig. 3. Qt-F-L ternary diagram of sandstones from the Nanpu Sag. Fields of various tectonic settings are from Dickinson *et al.* (1983).

sandstone samples were collected from these boreholes, and they were classified into 4 units according to their stratigraphic features, including Ed sandstones ( $n = 4$ ), Ngl sandstones ( $n = 9$ ), Ngu sandstones ( $n = 19$ ), Nm sandstones ( $n = 5$ ). The samples were analyzed under the microscope in thin sections. 400 points were counted for each sample using the traditional method of Dickinson and Suczek (1979) and Dickinson *et al.* (1983).

Whole-rock geochemistry analysis was carried out at the Laboratory of Isotope Geochronology and Geochemistry, Chinese Academy of Sciences. Each sample was powdered to 200 mesh in an agate mill to avoid contamination. Loss of ignition (LOI) was determined at 900°C for 90 min. Fused-glass discs were prepared for major element analysis by X-ray fluorescence method as described in detail by Ahmedali (1989). The analytical precision is better than 5% for major elements. Trace element data, including rare earth elements (REE), were obtained with standard ICP-MS procedures as described in detail by Jenner *et al.* (1990). Accuracy and precision was estimated and monitored from the control samples and duplicates. The precision of replicate analysis is better than 5% for all analyzed trace elements except Zn, Ga and V, which have precisions of 5–8%.

## RESULTS

### Petrography

Summary results of modal analysis for sandstone samples are shown in Table 1. Most samples are feldspathic litharenite and litharenite, along with a few lithic arkoses.

Table 2. Major element contents and their correlative ratios of sandstones in the Nanpu Sag

Sample	Minghuazhen Formation (Nm, $n = 5$ )							The upper member of Guantao Formation (Ngu, $n = 19$ )						
	B14-4	B14-7	NP1-1 <sup>†</sup>	NP1-2	B14-8 <sup>†</sup>	B14-10	B14-12	B14-13	B14-15	B14-16	B14-17	L25-8	L25-9	
Depth/m	1657.80	1665.30	1827.90	1831.00	1678.68	1890.60	1895.87	1898.10	1905.37	1908.00	1911.20	1919.60	1922.20	
SiO <sub>2</sub>	72.35	72.14	71.56	78.77	68.43	72.81	78.96	76.87	77.47	80.14	75.21	80.45	69.01	
Al <sub>2</sub> O <sub>3</sub>	13.28	13.41	13.91	11.31	13.89	12.26	10.83	11.52	10.88	9.74	10.94	10.69	13.97	
CaO	1.10	0.96	1.28	0.85	1.13	1.00	0.64	0.76	0.86	0.81	0.88	0.37	1.02	
Fe <sub>2</sub> O <sub>3</sub> *	3.27	3.82	3.18	1.52	4.07	4.71	1.71	2.03	2.23	2.44	4.61	1.43	6.19	
K <sub>2</sub> O	3.40	3.23	3.45	2.97	3.24	2.97	3.07	3.34	3.12	2.49	3.00	3.36	3.10	
MgO	1.06	1.18	1.15	0.45	1.49	0.75	0.54	0.68	0.57	0.60	0.85	0.31	1.35	
MnO	0.04	0.05	0.04	0.01	0.05	0.09	0.02	0.03	0.04	0.04	0.09	0.01	0.04	
Na <sub>2</sub> O	2.83	2.55	3.15	2.77	3.40	2.03	2.30	2.72	2.31	1.92	2.23	1.93	1.92	
P <sub>2</sub> O <sub>5</sub>	0.07	0.05	0.08	0.04	0.08	0.05	0.04	0.04	0.04	0.06	0.05	0.03	0.07	
TiO <sub>2</sub>	0.38	0.42	0.41	0.13	0.53	1.23	0.27	0.21	0.26	0.35	0.28	0.17	0.61	
LOI	2.14	2.10	1.69	1.05	3.66	2.03	1.51	1.71	2.75	1.39	1.77	1.14	2.68	
Total	99.92	99.91	99.90	99.87	99.97	99.93	99.89	99.91	100.53	99.98	99.91	99.89	98.96	
ClA	56.20	58.66	55.27	54.80	55.43	59.39	56.67	54.85	55.42	57.04	56.20	58.78	62.50	
SiO <sub>2</sub> /Al <sub>2</sub> O <sub>3</sub>	5.45	5.38	5.14	6.96	4.93	5.94	7.29	6.67	7.12	8.23	6.87	7.53	4.94	
K <sub>2</sub> O/Na <sub>2</sub> O	1.20	1.27	1.10	1.07	0.95	1.46	1.36	1.23	1.35	1.30	1.35	1.745	1.61	
MgO+Fe <sub>2</sub> O <sub>3</sub>	4.33	5.00	4.33	1.97	5.56	5.46	2.25	2.71	2.80	3.04	5.46	1.74	7.54	
Al <sub>2</sub> O <sub>3</sub> /(CaO+Na <sub>2</sub> O)	3.38	3.84	3.14	3.12	3.07	4.05	3.68	3.31	3.43	3.57	3.52	4.65	4.75	

The upper member of Guantao Formation (Ngu, n = 19)

Sample	The upper member of Guantao Formation (Ngu, n = 19)													
	NPI-5	B32X1-26	B32X1-21	B32X1-14	B32X1-13 <sup>†</sup>	B32X1-12	B32X1-11 <sup>†</sup>	B32X1-10	B32X1-9	B32X1-6	B32X1-5			
Depth/m	1902.42	2045.27	2052.60	2061.10	2065.20	2068.00	2069.60	2070.00	2072.68	2076.80	2078.10			
SiO <sub>2</sub>	74.89	79.54	80.22	72.03	67.18	72.58	74.17	74.86	75.43	69.3	81.83			
Al <sub>2</sub> O <sub>3</sub>	12.51	10.55	10.04	13.90	15.69	13.54	11.68	12.53	11.71	13.93	9.47			
CaO	1.07	0.78	0.77	1.58	1.94	1.27	0.61	0.67	0.87	0.95	0.33			
Fe <sub>2</sub> O <sub>3</sub> *	2.74	1.93	2.28	3.60	5.22	3.17	3.24	3.16	3.12	5.55	1.94			
K <sub>2</sub> O	3.15	3.01	2.85	3.33	2.95	3.19	2.86	2.90	3.13	3.22	3.29			
MgO	0.91	0.50	0.51	0.74	1.09	0.79	0.89	1.00	0.60	1.36	0.28			
MnO	0.02	0.01	0.02	0.03	0.04	0.03	0.02	0.02	0.02	0.03	0.02			
Na <sub>2</sub> O	2.75	1.79	1.74	2.59	2.61	2.82	3.60	1.45	2.62	2.37	1.38			
P <sub>2</sub> O <sub>5</sub>	0.06	0.04	0.04	0.09	0.11	0.08	0.02	0.02	0.06	0.06	0.03			
TiO <sub>2</sub>	0.35	0.26	0.21	0.32	0.59	0.27	0.59	0.72	0.34	0.59	0.14			
LOI	1.42	1.49	1.29	1.91	2.59	2.20	2.29	2.61	2.01	2.56	1.20			
Total	99.87	99.90	99.97	100.12	100.01	99.94	99.97	99.94	99.91	99.92	99.91			
ClA	55.85	58.03	57.71	56.38	58.72	56.52	53.54	64.98	55.76	60.42	59.52			
SiO <sub>2</sub> /Al <sub>2</sub> O <sub>3</sub>	5.99	7.54	7.99	5.18	4.28	5.36	6.35	5.97	6.44	4.97	8.64			
K <sub>2</sub> O/Na <sub>2</sub> O	1.15	1.68	1.64	1.29	1.13	1.13	0.79	2.00	1.19	1.36	2.38			
MgO+Fe <sub>2</sub> O <sub>3</sub>	3.65	2.43	2.79	4.34	6.31	3.96	4.13	4.16	3.72	6.91	2.22			
Al <sub>2</sub> O <sub>3</sub> /(CaO+Na <sub>2</sub> O)	3.27	4.11	4.00	3.33	3.45	3.31	2.77	5.91	3.36	4.20	5.54			

Sample	The lower member of Guantao Formation (Ngl, n = 9)											Dongying Formation (Ed, n = 4)			
	L25-10	L25-11	L25-12	B32X1-4	B32X1-3	B32X1-2	B32X1-1	NPI-4	NPI-6	NPI-8	NPI-9	NPI-10	NPI-11		
Depth/m	2058.35	2063.30	2065.78	2391.80	2395.30	2398.22	2401.50	2390.85	2393.50	2482.50	2624.20	2628.45	2631.15		
SiO <sub>2</sub>	77.57	82.66	79.61	82.79	74.42	81.33	79.03	72.09	78.41	71.68	65.36	71.82	78.00		
Al <sub>2</sub> O <sub>3</sub>	10.05	9.27	9.79	9.56	12.79	10.85	8.31	8.70	9.13	9.92	11.76	10.08	8.63		
CaO	0.21	0.17	0.26	0.24	0.35	0.37	0.33	1.85	1.16	2.65	3.64	3.17	2.14		
Fe <sub>2</sub> O <sub>3</sub> *	1.39	1.31	2.11	1.24	3.53	0.75	4.63	5.86	2.92	3.73	4.36	2.66	1.50		
K <sub>2</sub> O	2.97	2.72	3.08	2.41	3.28	2.75	2.42	2.44	2.57	2.46	2.86	2.67	2.49		
MgO	0.46	0.39	0.43	0.3	0.42	0.28	0.51	1.32	0.80	1.45	2.14	1.75	1.24		
MnO	0.01	0.01	0.01	0.01	0.04	0.01	0.04	0.07	0.05	0.08	0.07	0.04	0.02		
Na <sub>2</sub> O	1.76	1.57	1.26	0.62	0.83	0.72	0.85	1.58	1.76	2.56	2.20	1.88	1.69		
P <sub>2</sub> O <sub>5</sub>	0.02	0.02	0.01	0.05	0.07	0.06	0.04	0.06	0.06	0.09	0.13	0.08	0.06		
TiO <sub>2</sub>	0.19	0.17	0.21	0.25	0.28	0.34	0.18	0.24	0.17	0.32	0.51	0.28	0.25		
LOI	1.51	1.60	3.13	2.42	3.94	2.46	3.65	6.03	2.87	5.21	6.98	5.57	4.01		
Total	100.21	99.89	99.90	99.89	99.95	99.92	99.99	100.24	99.90	100.15	100.01	100.00	100.03		
ClA	60.72	61.33	62.44	70.13	69.69	69.14	64.24	50.24	53.94	45.87	46.83	46.15	47.92		
SiO <sub>2</sub> /Al <sub>2</sub> O <sub>3</sub>	7.72	8.92	8.13	8.66	5.82	7.50	9.51	8.29	8.59	7.23	5.56	7.13	9.04		
K <sub>2</sub> O/Na <sub>2</sub> O	1.69	1.73	2.44	3.89	3.95	3.82	2.85	1.54	1.46	0.96	1.30	1.42	1.47		
MgO+Fe <sub>2</sub> O <sub>3</sub>	1.85	1.70	2.54	1.54	3.95	1.03	5.14	7.18	3.72	5.18	6.50	4.41	2.73		
Al <sub>2</sub> O <sub>3</sub> /(CaO+Na <sub>2</sub> O)	5.11	5.33	6.44	11.11	10.84	9.95	7.04	2.54	3.13	1.90	2.01	2.00	2.25		

Fe<sub>2</sub>O<sub>3</sub>\* = total Fe expressed as Fe<sub>2</sub>O<sub>3</sub>.

† Shows greywacke.

Table 3. Trace element contents and their correlative ratios of sandstones in the Nanpu Sag

Samples	Minghuazhen Formation (Nim, n = 5)					The upper member of Guangtao Formation (Ngu, n = 19)									
	B14-4	B14-7	NPI-1 <sup>†</sup>	NPI-2	B14-8 <sup>‡</sup>	B14-10	B14-12	B14-13	B14-15	B14-16	B14-17	L25-8	L25-9	NPI-5	
Sc	5.50	6.68	6.18	2.13	8.59	9.60	3.83	4.27	4.25	4.54	4.73	2.62	2.50	5.00	
V	51.50	58.12	48.97	17.28	69.61	77.51	30.45	30.21	32.10	25.81	33.87	21.37	20.49	44.33	
Cr	66.45	67.43	58.15	17.92	81.98	74.07	26.32	33.00	26.34	23.82	31.52	22.30	28.34	46.32	
Co	8.79	9.55	8.45	4.03	14.19	32.37	8.19	6.56	6.15	6.18	7.21	4.64	4.36	9.45	
Ni	22.91	24.86	20.85	8.10	29.31	73.96	11.53	14.34	7.79	7.64	10.60	7.70	11.21	16.93	
Rb	100.60	93.99	95.92	72.11	100.60	96.74	86.20	98.70	95.22	80.07	90.90	98.14	93.52	85.83	
Cs	1.85	2.64	1.87	0.83	2.80	2.34	1.63	1.86	1.84	1.74	1.67	1.50	1.52	1.56	
Ba	1016.6	849.9	1134.8	896.6	885.3	634.9	650.1	708.7	1328.4	637.8	817.8	784.3	755.5	957.5	
Zr	311.9	270.2	305.5	280.2	302.2	233.4	175.3	219.7	727.5	182.7	286.0	151.4	133.3	293.5	
Sr	102.9	116.5	117.6	66.7	147.2	72.8	197.7	60.5	87.1	355.9	94.7	79.4	50.7	98.4	
Y	11.21	12.51	9.88	5.86	13.75	24.42	9.67	9.70	10.65	13.24	10.55	7.92	7.33	9.95	
Nb	8.36	8.64	8.81	4.25	11.16	18.81	5.09	4.80	5.30	6.36	5.42	4.00	3.31	8.36	
Hf	2.88	3.22	3.20	1.86	3.96	10.9	2.15	1.80	2.60	4.76	2.81	2.26	1.59	2.75	
Ta	0.61	0.64	0.62	0.32	0.81	1.51	0.45	0.43	0.47	0.64	0.49	0.35	0.29	0.62	
Pb	16.81	22.26	22.80	12.79	21.22	21.34	17.11	19.93	18.93	16.84	18.96	18.16	17.17	16.10	
Th	5.31	7.51	6.20	2.90	7.07	18.78	5.24	5.52	5.09	4.89	5.70	4.34	3.70	4.75	
U	1.20	1.82	0.861	0.759	2.19	4.36	1.43	1.25	1.18	1.91	1.15	0.91	0.87	1.51	
La	25.06	30.18	26.49	16.16	35.35	47.56	18.27	19.63	18.57	20.25	21.33	16.46	13.50	25.37	
Ce	46.96	62.58	51.06	28.91	67.71	100.50	38.89	41.89	38.47	45.48	44.77	33.62	28.06	49.47	
Pr	5.81	7.22	6.41	3.55	8.31	12.5	4.56	5.03	4.59	4.92	5.17	4.05	3.24	5.78	
Nd	20.30	24.66	21.79	11.67	28.72	42.85	15.70	17.14	16.31	18.52	18.06	13.79	11.32	19.58	
Sm	3.36	4.09	3.62	1.85	4.59	7.56	2.74	3.08	3.05	3.24	3.15	2.41	1.98	3.20	
Eu	0.79	0.88	0.74	0.53	1.03	1.20	0.67	0.70	0.64	0.76	0.69	0.57	0.49	0.74	
Gd	2.34	2.76	2.38	1.21	3.18	5.56	2.17	2.20	2.31	2.60	2.27	1.74	1.55	2.15	
Tb	0.39	0.47	0.37	0.20	0.50	0.83	0.35	0.36	0.36	0.43	0.36	0.28	0.26	0.35	
Dy	2.18	2.52	2.02	1.16	2.73	4.73	1.90	2.01	2.09	2.52	2.11	1.58	1.43	2.01	
Ho	0.45	0.48	0.39	0.23	0.55	0.98	0.39	0.39	0.44	0.54	0.42	0.31	0.28	0.39	
Er	1.16	1.33	1.16	0.64	1.50	2.80	1.10	1.04	1.21	1.49	1.19	0.891	0.823	1.12	
Tm	0.18	0.21	0.18	0.10	0.22	0.45	0.17	0.16	0.19	0.25	0.18	0.14	0.13	0.17	
Yb	1.16	1.25	1.11	0.640	1.40	3.06	1.09	1.02	1.23	1.71	1.23	0.934	0.858	1.06	
Lu	0.17	0.19	0.16	0.10	0.21	0.48	0.16	0.15	0.18	0.25	0.18	0.13	0.13	0.16	
Ce/Ce*	0.94	1.02	0.94	0.92	0.95	0.99	1.03	1.01	1.00	1.10	1.03	0.99	1.02	0.98	
Eu/Eu*	0.86	0.80	0.77	1.08	0.82	0.57	0.84	0.82	0.74	0.80	0.79	0.85	0.86	0.86	
ΣREE	110.32	138.82	117.88	66.95	155.98	231.00	88.17	94.80	89.63	102.97	101.10	76.91	64.05	111.55	
L/H	12.74	14.09	14.19	14.68	14.18	11.23	11.03	11.93	10.20	9.50	11.75	11.80	10.73	14.05	
(La/Yb) <sub>N</sub>	14.63	16.23	16.09	17.02	17.01	10.49	11.27	12.95	10.17	7.97	11.67	11.88	10.61	16.20	
(Gd/Yb) <sub>N</sub>	1.64	1.77	1.73	1.52	1.83	1.47	1.60	1.74	1.52	1.23	1.48	1.50	1.46	1.64	
La/Sc	4.56	4.52	4.29	7.60	4.11	4.95	4.77	4.60	4.37	4.46	4.51	6.28	5.39	5.07	
Th/Sc	0.96	1.12	1.00	1.36	0.82	1.96	1.37	1.29	1.20	1.08	1.21	1.65	1.48	0.95	
Th/Co	0.60	0.79	0.73	0.72	0.50	0.58	0.64	0.84	0.83	0.79	0.79	0.94	0.85	0.50	
Th/Cr	0.08	0.11	0.11	0.16	0.09	0.25	0.20	0.17	0.19	0.21	0.18	0.19	0.13	0.10	
Th/U	4.43	4.13	7.21	3.82	3.23	4.31	3.66	4.42	4.31	2.56	4.96	4.77	4.25	3.15	

The upper member of Guangtao Formation (Ngu, n = 19)

Samples	The upper member of Guangtao Formation (Ngu, n = 19)									
	B32X1-26	B32X1-21	B32X1-14	B32X1-13 <sup>+</sup>	B32X1-12	B32X1-11 <sup>+</sup>	B32X1-10	B32X1-9	B32X1-6	B32X1-5
Sc	4.34	3.15	6.31	9.15	5.08	6.94	6.30	3.97	8.53	10.30
V	31.19	27.89	48.20	65.64	39.32	54.46	53.04	36.60	64.73	85.68
Cr	31.93	43.02	26.82	253.60	20.59	50.44	59.66	58.36	79.41	79.85
Co	7.98	11.24	9.58	11.80	7.02	8.16	8.49	6.57	17.28	11.81
Ni	10.21	15.75	12.80	155.20	8.33	15.27	24.41	22.92	26.88	24.07
Rb	84.70	78.55	91.10	82.80	85.68	94.14	85.56	81.07	104.70	109.70
Cs	1.47	1.35	1.55	1.58	1.39	3.33	3.01	1.34	3.51	4.04
Ba	852.8	815.8	1985.0	2016.5	1543.8	720.9	658.6	845.4	805.5	744.1
Sr	196.9	204.1	1180.3	1484.7	939.4	226.9	204.6	255.8	272.8	273.3
Zr	76.3	200.9	99.2	108.8	102.8	226.8	327.0	120.9	233.9	74.3
Y	9.34	8.36	13.00	14.25	12.14	13.96	14.33	11.58	19.23	19.30
Nb	4.26	4.11	5.72	7.83	5.08	11.06	11.64	8.18	14.26	15.67
Hf	2.41	2.29	3.06	3.35	3.15	6.74	9.40	3.74	6.72	5.89
Ta	0.42	0.36	0.49	0.63	0.46	0.92	0.87	0.65	1.09	1.18
Pb	21.41	17.80	22.93	22.32	21.61	27.77	21.97	16.38	23.34	24.53
Th	5.60	4.44	5.81	6.21	5.66	8.45	11.32	11.21	8.98	11.34
U	1.76	0.97	1.30	1.40	1.38	2.09	2.15	1.81	1.76	1.90
La	18.19	18.19	19.94	23.19	19.88	25.77	31.69	23.88	36.11	41.57
Ce	38.67	37.20	42.75	49.14	43.05	50.86	65.92	45.30	69.68	80.09
Pr	4.43	4.36	5.19	6.04	5.16	6.00	7.79	5.60	8.83	10.20
Nd	15.61	15.03	18.78	21.54	18.25	20.93	27.43	19.45	30.45	35.17
Sm	2.78	2.56	3.52	3.94	3.38	3.58	4.66	3.25	5.21	5.92
Eu	0.65	0.60	0.80	0.97	0.83	0.78	0.86	0.73	1.11	1.22
Gd	2.11	1.87	2.81	3.17	2.80	2.49	2.94	2.50	3.94	4.24
Tb	0.36	0.31	0.47	0.51	0.44	0.42	0.47	0.40	0.64	0.67
Dy	2.03	1.82	2.66	2.96	2.53	2.71	2.92	2.34	3.68	3.79
Ho	0.40	0.34	0.54	0.61	0.52	0.56	0.59	0.45	0.77	0.79
Er	1.12	0.978	1.47	1.65	1.46	1.65	1.69	1.30	2.12	2.18
Tm	0.17	0.15	0.24	0.26	0.22	0.26	0.27	0.20	0.33	0.34
Yb	1.14	0.99	1.45	1.64	1.41	1.77	1.82	1.32	2.17	2.17
Lu	0.16	0.14	0.21	0.25	0.21	0.28	0.28	0.20	0.33	0.35
Ce/Ce*	1.04	1.01	1.01	1.00	1.02	0.98	1.01	0.94	0.94	0.94
Eu/Eu*	0.82	0.84	0.78	0.84	0.82	0.80	0.71	0.78	0.75	0.74
ΣREE	87.81	84.55	100.82	115.87	100.13	118.08	149.32	106.91	165.37	188.72
L/H	10.73	11.79	9.24	9.49	9.45	10.63	12.60	11.29	10.83	11.98
(La/Yb) <sub>N</sub>	10.74	12.34	9.26	9.53	9.52	9.80	11.73	12.16	11.24	12.89
(Gd/Yb) <sub>N</sub>	1.49	1.52	1.56	1.56	1.60	1.13	1.30	1.52	1.47	1.57
La/Sc	4.19	5.77	3.16	2.53	3.91	3.71	5.03	6.01	4.23	4.03
Th/Sc	1.29	1.41	0.92	0.68	1.12	1.22	1.80	2.82	1.05	1.10
Th/Co	0.70	0.40	0.61	0.53	0.81	1.04	1.33	1.71	0.52	0.96
Th/Cr	0.18	0.10	0.22	0.02	0.27	0.17	0.19	0.19	0.11	0.14
Th/U	3.18	4.58	4.47	4.44	4.10	4.04	5.27	6.19	5.10	5.97

Table 3. (continued)

Samples	The lower member of Guangtao Formation (Ngl, n = 9)									Dongying Formation (Ed, n = 4)			
	L25-10	L25-11	L25-12	B32X1-4	B32X1-3	B32X1-2	B32X1-1	NPI-4	NPI-6	NPI-8	NPI-9	NPI-10	NPI-11
Sc	3.18	2.87	3.74	2.06	4.33	2.33	4.38	5.60	2.64	5.20	5.32	2.92	3.13
V	24.63	23.24	47.71	23.56	38.77	25.78	33.22	53.49	23.93	44.34	49.97	30.76	27.14
Cr	29.43	25.99	42.26	28.08	50.68	51.59	23.09	32.19	16.34	37.58	43.57	22.25	22.97
Co	3.26	5.84	5.63	4.61	6.22	3.96	5.40	5.80	3.89	7.22	8.11	5.03	5.65
Ni	8.50	9.57	7.62	9.50	17.69	12.38	13.95	12.46	8.03	14.72	18.94	8.99	11.37
Rb	83.30	73.51	85.29	66.67	93.29	73.80	66.79	66.09	62.54	72.52	77.44	70.45	64.82
Cs	1.37	1.13	1.79	0.92	1.11	0.83	0.81	1.22	0.90	1.64	1.41	1.09	1.06
Ba	843.7	742.3	882.2	2145.7	877.8	705.7	704.8	607.8	603.6	729.8	888.1	794.3	727.5
Sr	131.8	123.0	131.9	80.1	122.1	97.8	88.3	157.1	143.7	195.6	217.7	202.0	160.0
Zr	68.4	66.9	115.6	162.2	139.8	131.6	114.3	186.6	111.0	123.7	187.0	71.6	97.9
Y	8.10	7.93	8.22	10.34	10.84	9.74	10.26	12.31	9.82	13.99	12.76	9.23	11.17
Nb	3.84	3.57	4.24	9.95	9.69	9.40	7.37	8.63	7.22	9.26	11.32	7.62	6.77
Hf	2.04	1.92	3.25	4.66	3.84	3.59	3.07	4.72	2.95	3.36	5.09	2.02	2.60
Ta	0.40	0.34	0.48	0.79	0.77	0.66	0.56	0.67	0.55	0.64	0.87	0.53	0.53
Pb	18.32	15.69	17.83	12.51	18.15	13.55	10.95	14.47	10.63	16.12	17.55	15.07	14.76
Th	5.79	4.98	5.08	6.12	5.97	5.32	4.82	4.88	4.36	5.52	6.69	4.42	4.60
U	1.28	1.39	1.81	1.30	2.33	1.90	1.14	1.18	0.99	1.32	1.26	0.849	1.06
La	17.60	16.43	15.87	24.62	26.44	22.38	22.03	26.79	22.42	30.54	32.39	24.63	25.72
Ce	33.68	35.79	34.85	45.79	49.49	41.92	41.78	51.89	44.33	57.80	62.04	47.27	49.72
Pr	4.00	4.17	3.72	5.27	6.30	5.38	5.14	6.18	5.15	6.83	7.30	5.78	6.06
Nd	13.75	14.88	12.82	18.69	21.51	17.78	17.39	20.78	17.31	23.38	26.99	19.62	20.44
Sm	2.33	2.68	2.40	2.99	3.50	2.95	2.93	3.50	2.90	3.89	4.34	3.13	3.26
Eu	0.51	0.61	0.54	0.37	0.74	0.54	0.54	0.72	0.55	0.80	0.92	0.72	0.68
Gd	1.70	1.90	1.73	2.02	2.36	1.95	2.07	2.41	1.98	2.82	2.97	2.00	2.40
Tb	0.27	0.31	0.30	0.35	0.37	0.35	0.35	0.41	0.31	0.44	0.45	0.34	0.37
Dy	1.61	1.68	1.68	2.02	2.22	1.99	1.97	2.35	1.88	2.55	2.56	1.88	2.23
Ho	0.31	0.32	0.33	0.41	0.44	0.40	0.40	0.49	0.38	0.52	0.51	0.35	0.44
Er	0.89	0.86	0.90	1.15	1.26	1.10	1.19	1.40	1.09	1.43	1.40	0.95	1.20
Tm	0.13	0.13	0.14	0.18	0.19	0.17	0.17	0.23	0.17	0.23	0.23	0.15	0.18
Yb	0.89	0.78	0.907	1.21	1.24	1.16	1.15	1.51	1.08	1.45	1.49	0.942	1.16
Lu	0.13	0.12	0.14	0.17	0.19	0.16	0.17	0.23	0.16	0.20	0.22	0.14	0.17
Ce/Ce*	0.97	1.04	1.09	0.97	0.92	0.92	0.94	0.97	0.99	0.96	0.97	0.95	0.96
Eu/Eu*	0.78	0.83	0.81	0.46	0.79	0.73	0.67	0.76	0.70	0.74	0.78	0.87	0.74
ΣREE	77.79	80.65	76.34	105.24	116.25	98.24	97.29	118.89	99.71	132.87	143.82	107.89	114.03
L/H	12.13	12.23	11.45	12.99	13.05	12.52	12.01	12.17	13.16	12.78	13.62	15.00	13.00
(La/Yb) <sub>N</sub>	13.35	14.20	11.80	13.70	14.33	13.03	12.88	11.99	14.03	14.22	14.71	17.63	14.94
(Gd/Yb) <sub>N</sub>	1.54	1.96	1.54	1.34	1.53	1.36	1.45	1.29	1.48	1.57	1.61	1.71	1.67
La/Sc	5.53	5.72	4.24	11.94	6.11	9.61	5.03	4.78	8.49	5.87	6.09	8.44	8.21
Th/Sc	1.82	1.73	1.36	2.97	1.38	2.28	1.10	0.87	1.65	1.06	1.26	1.51	1.47
Th/Co	1.78	0.85	0.90	1.33	0.96	1.34	0.89	0.84	1.12	0.76	0.82	0.88	0.81
Th/Cr	0.20	0.19	0.12	0.22	0.12	0.10	0.21	0.15	0.27	0.15	0.15	0.20	0.20
Th/U	4.52	3.58	2.81	4.71	2.56	2.80	4.23	4.14	4.40	4.18	5.31	5.20	4.34

$$L/H = \Sigma LREE/\Sigma HREE, LREE: La-Eu; HREE: Gd-Lu. Ce/Ce^* = Ce_N/(La_N * Pr_N)^{1/2}, Eu/Eu^* = Eu_N/(Sm_N * Gd_N)^{1/2}.$$

† Shows greywacke.

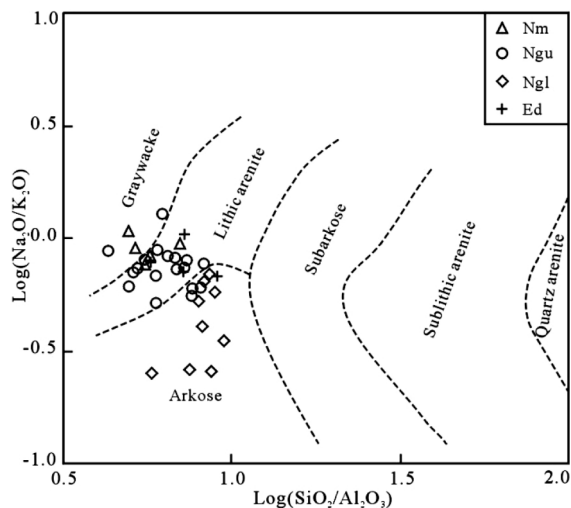


Fig. 4. Geochemical classification of sandstones from the Nanpu Sag using the  $\log(\text{Na}_2\text{O}/\text{K}_2\text{O})$  vs.  $\log(\text{SiO}_2/\text{Al}_2\text{O}_3)$  diagram (after Pettijohn *et al.*, 1973).

Generally, matrix and cement mineral constitutes up to 9–23% of the total rock volume. The framework grains are moderate in size, angular to subangular in shape, and poorly to moderately sorted. Grain-support and contact-cement textures are frequently observed in most samples. The minerals recorded are monocrystalline quartz (Qm), polycrystalline quartz (Qp), plagioclase (P), alkali feldspar (AF, including orthoclase and microcline), lithic sedimentary and metasedimentary clasts (Ls), and lithic volcanic clasts (Lv). Ls and Lv constitute the lithic clastics (L) and together with Qp the total lithic clastics (Lt), Qm and Qp make together total quartz (Qt). Furthermore detrital zircon, biotite, apatite and other heavy minerals (H) are also distinguished.

All samples have relatively high quartz (Qt) contents of 34–60%, and each group (Es–Nm) has an average content of 37.3%, 53.3%, 50.2%, and 53%. Monocrystalline quartz is much commoner than polycrystalline quartz. Potassium feldspar usually dominates over plagioclase. Felsic volcanic grains and granites mainly dominate the lithic fragments in sandstones, whereas sedimentary and metasedimentary grains are rare. Accordingly, The ratios of detrital Qt: F: L modes considered group by group are as follows:  $51 \pm 5:31 \pm 5:18 \pm 5$  (Ed);  $68 \pm 5:20 \pm 4:12 \pm 5$  (Ngl);  $63 \pm 7:24 \pm 5:13 \pm 5$  (Ngu);  $57 \pm 5:28 \pm 4:15 \pm 5$  (Nm) (Table 1).

On a Qt–F–L ternary diagram (Fig. 3), the Nanpu Sag sandstones show a grouping of data in the recycled orogenic provenance field and a subordinate continental block field, indicating an uplifted continental fragment as a likely source area. Paleocurrent data suggest that this exposed land was located north of the study area (Wang, H. *et al.*, 2002).

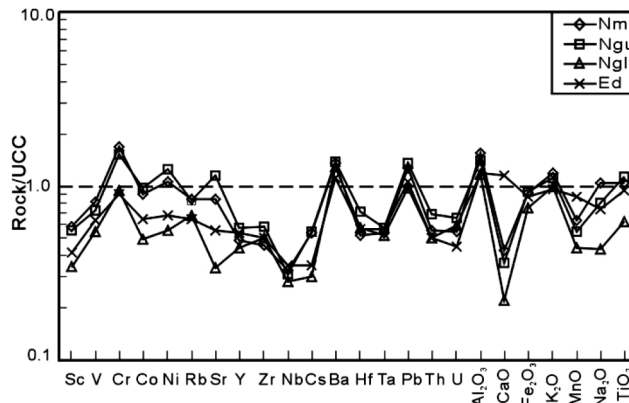


Fig. 5. Multi-element normalized diagram for the Nanpu Sag sandstones, normalized against average upper continental crust (Taylor and McLennan, 1985).

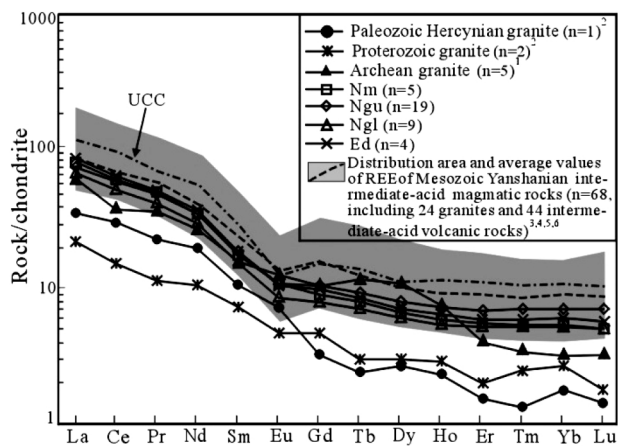


Fig. 6. REE distribution patterns of Middle Oligocene–Pliocene sandstones from the Nanpu Sag and of felsic magmatic rocks in the Yanshan Fold Belt. REE data of CI chondrite-normalization are from Boynton (1984). Numbers 1–5 are represented by references respectively as follows: 1: Xiao *et al.*, 1994; 2: Tan, 1997; 3: Xu *et al.*, 1999; 4: Li, W. P., 2003; 5: Li, X. Y., 2003; 6: Wang, Q. *et al.*, 2002.

### Geochemistry

The major-element and trace element concentrations of all the Nanpu Sag sandstones are arranged in Table 2 and Table 3 respectively according to their sedimentary sequences.

**Major elements** Generally, these sandstones are characterized by moderate contents of  $\text{SiO}_2$  (65.36–82.79%, average  $75.43 \pm 4.57\%$ ) and  $\text{Al}_2\text{O}_3$  (8.31–15.69%,  $11.41 \pm 1.90\%$ ), and low contents of  $\text{Fe}_2\text{O}_3^* + \text{MgO}$  (1.04–7.54%,  $3.89 \pm 1.71\%$ ) and  $\text{TiO}_2$  (0.13–1.23%,  $0.35 \pm 0.21\%$ ), due to their high quartz contents and lesser mafic components. The low CaO contents (0.17–3.64%,  $1.05 \pm$

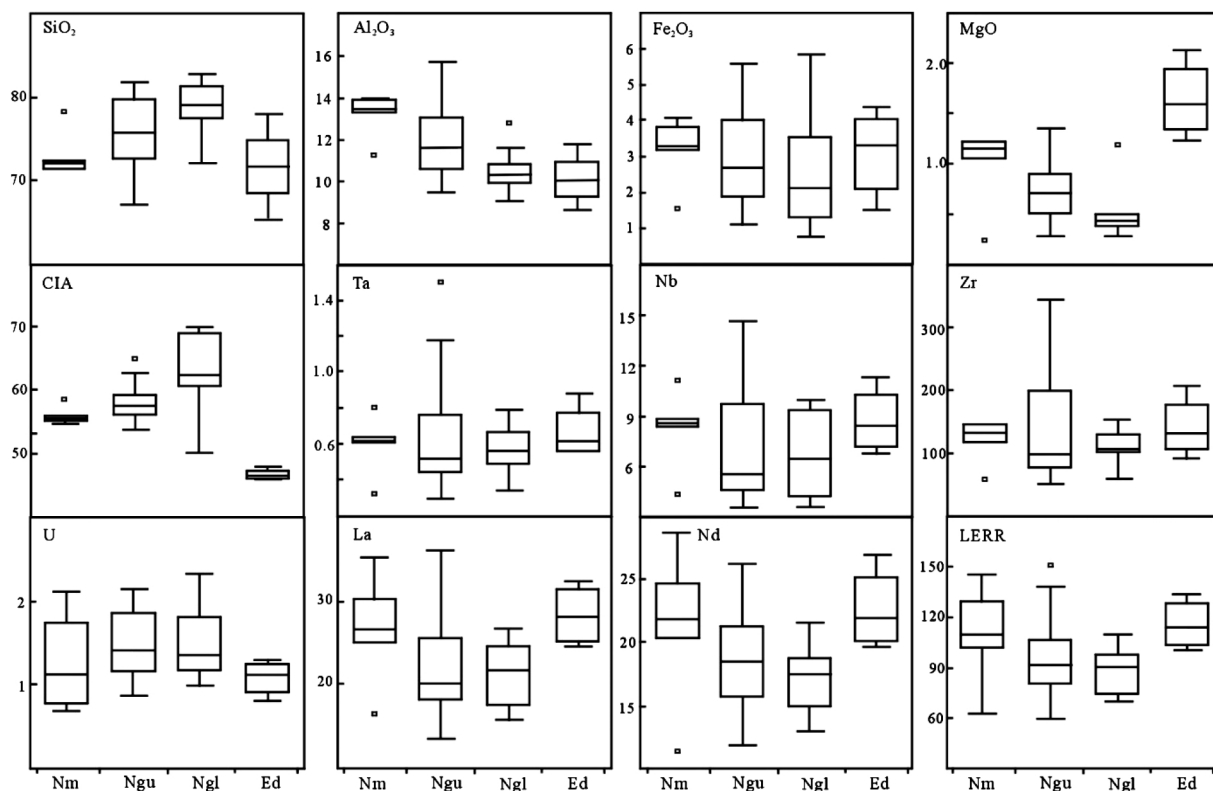


Fig. 7. Box-and-whisker plots of sandstone compositions of the Nanpu Sag showing that there are three divisions in the data sets: first part = Ed sandstones; second part = Ngl + Ngu sandstones; third part = Nm sandstones (modified after Liu *et al.*, 2006a).

0.80%) indicate that all the sandstones have very low carbonate component. The moderate negative correlation ( $r = -0.66$ ) between  $\text{SiO}_2$  and CaO may suggest that both the detrital and the matrix carbonate in all the samples are primary rather than secondary, because the influence of secondary carbonate could result in  $\text{SiO}_2$ -CaO scatter (Feng and Kerrich, 1990). Compared with the compositions of different clastic rock types, it is clear that major element contents (e.g.,  $\text{SiO}_2$ ,  $\text{Al}_2\text{O}_3$ ,  $\text{Fe}_2\text{O}_3^*$ , MgO, and  $\text{TiO}_2$ ) and key ratios (e.g.,  $\text{SiO}_2/\text{Al}_2\text{O}_3$ , and  $\text{Al}_2\text{O}_3/(\text{Na}_2\text{O} + \text{CaO})$ ) obviously differ from those of graywackes, but are similar to those of arkose and lithic arenite. In the geochemical classification diagram of Pettijohn *et al.* (1973) the studied sandstones plot in the litharenite and arkose fields, except for four samples that fall in the greywacke area (Fig. 4). This classification is generally consistent with the petrologic data. In general, most samples show clearly depletion of CaO and MnO relative to upper continental crust (UCC) (Taylor and McLennan, 1985), and also slightly enrichment of  $\text{Al}_2\text{O}_3$  (Fig. 5).

**Trace elements** The contents of Rb, Ba, Cs and Sr in the sandstones from Nanpu Sag vary to a great degree from 62.54 to 109.70 ppm, 603.6 to 2145.7 ppm, 0.81 to 4.04 ppm, 80.1 to 1484.7 ppm, respectively. Compared with UCC (Taylor and McLennan, 1985), Rb, Cs and Sr are

distinctly depleted whereas Ba is weakly enriched (Fig. 5).

The contents of Cr, Co, Ni and Sc show a wide range from 16.34 to 253.60 ppm, 3.26 to 32.37 ppm, 7.62 to 155.20 ppm, 2.06 to 10.30 ppm respectively. Only a few samples (e.g., B14-10) have relatively high contents, suggesting a contribution from more mafic components.

Contents of the High field strength elements Th, Y, Nb, Ta show a similarly wide ranges from 2.90 to 18.78 ppm, 5.86 to 24.42 ppm, 3.31 to 18.81 ppm, 0.29 to 1.51 ppm respectively. Compared to UCC, the concentrations of most high field strength elements are generally low and average relative ratios lie between 0.2 and 0.7. Zr and Hf are somewhat depleted compared to the UCC (Fig. 5).

**Rare earth elements** The absolute concentrations of  $\Sigma\text{REE}$  vary greatly (64.05–231.00 ppm, average  $111.80 \pm 33.89$  ppm). As a whole, the chondrite-normalized patterns of the Nanpu Sag sandstones are similar to that of UCC, with distinctive negative Eu-anomalies (0.46–1.08, average  $0.78 \pm 0.09$ ), LREE (La–Eu) enrichment [ $(\text{La}/\text{Yb})_{\text{N}} = 7.97$ –17.63,  $12.82 \pm 2.41$ ] and flat HREE (Gd–Lu) [ $(\text{Gd}/\text{Yb})_{\text{N}} = 1.13$ –1.96,  $1.54 \pm 0.16$ ]. All samples lack obvious Ce-anomalies (0.92–1.10,  $0.99 \pm 0.04$ ) (Fig. 6).

**Geochemical variation of stratigraphy** Stratigraphic trends in geochemistry are more difficult to recognize, although there are some stratigraphic variations existing. Liu *et al.* (2006a) used element box-and-whisker plots of the Nanpu Sag sandstones to facilitate geochemical data interpretation. In Fig. 7, it is clear that the trends of these variables (the contents of elements or various key parameters) can be divided into three time periods. The first part is the Middle–Late Oligocene (Ed Formation) sandstones, which is characterized by low  $\text{SiO}_2$  contents ( $71.72 \pm 5.16\%$ ), small CIA values ( $46.69 \pm 0.91$ ), and abundant  $\text{Fe}_2\text{O}_3$  ( $3.06 \pm 1.26\%$ ) and  $\text{MgO}$  contents ( $1.65 \pm 0.39\%$ ) as well as other element contents (e.g., Ta, Zr, La). The second part is the Miocene (Ng Formation, consists of Ngl member and Ngu member) sandstones, differing from the first one, it is characterized by relatively higher contents of  $\text{SiO}_2$  ( $76.46 \pm 4.26\%$ ) and higher CIA ( $59.29 \pm 4.92$ ) values, and lower contents of  $\text{Fe}_2\text{O}_3$  ( $3.04 \pm 1.51\%$ ) and  $\text{MgO}$  ( $0.69 \pm 0.32\%$ ). The third part is the Pliocene (Nm Formation) sandstones, which has the characterization of relatively lower  $\text{SiO}_2$  ( $72.65 \pm 3.77\%$ ) contents and CIA ( $56.07 \pm 1.53$ ) values, and higher  $\text{Fe}_2\text{O}_3$  ( $3.17 \pm 1.00\%$ ) and  $\text{MgO}$  ( $1.07 \pm 0.38\%$ ) contents than those of the second part. In most cases, the differences in the variables between these three parts are larger than the variations within each part.

## DISCUSSION

### *Effect of hydraulic sorting and quartz dilution*

It is widely accepted that hydraulic sorting and quartz dilution can significantly influence the chemical composition of terrigenous sediments, thus sorting and concentration of accessory minerals is especially important in the coarser rocks, with zircon, monazite and apatite usually affecting the distribution of some trace elements (Cullers, 1994a, 2000). Irregular change of Zr content, Zr/Th and Zr/Yb ratios in the Nanpu Sag sandstones show that zircon accumulation is not an important process and poor Zr–Th ( $r = 0.14$ ) and Zr–REEs ( $r = 0.20$ ) correlations indicate that zircon has little influence over the abundance of these elements. The limited grain-size variation (0.45–0.25 mm) and moderate clay proportions (generally <15%) observed by microscopic analysis in these sandstone thin sections show that quartz dilution should have slight influence over the chemical composition of these samples. This is consistent with the poor correlations between  $\text{SiO}_2$  and some other elements, such as  $\text{SiO}_2$ –Th ( $r = -0.17$ ) and  $\text{SiO}_2$ –REEs ( $r = -0.37$ ).

### *Sediment maturity and weathering*

Modal mineralogical analyses show that quartz/total feldspar ratios of the Nanpu Sag sandstones range from 1.31 to 6.11, with an average value of  $2.72 \pm 0.98$ , sug-

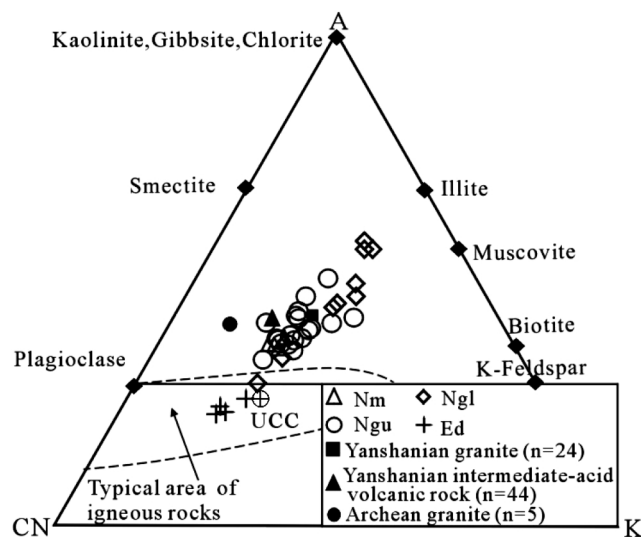


Fig. 8.  $\text{Al}_2\text{O}_3$  (A)– $\text{CaO}^* + \text{Na}_2\text{O}$  (CN)– $\text{K}_2\text{O}$  (K) ternary plot (after Nesbitt and Young, 1984;  $\text{CaO}^*$  is silicate CaO) of the Nanpu Sag sandstones calculated as molar proportions.

gesting low to moderate chemical weathering of these units. In contrast, the sandstones of the Ng Formation have a higher quartz/total feldspar ratio than those of the Ed Formation and the Nm Formation (Table 1). This suggests that detritus in the Ng Formation was weathered relatively enough to have removed more of the feldspar from the original sources than in the other two formations. This variational trend will be seen to be consistent with the chemical index of weathering of these units as discussed later.

The  $\text{SiO}_2/\text{Al}_2\text{O}_3$  ratio is sensitive to sediment recycling and weathering process, and can be used as a signal of sediment maturity, increasing as quartz survives preferentially to feldspars, mafic minerals and lithic grains (Roser and Korsch, 1986; Roser *et al.*, 1996). Average values in unaltered igneous rocks range from  $\sim 3.0$  (basic) to  $\sim 5.0$  (acidic), while values  $>5.0$ – $6.0$  in sediments are an indication of progressive maturity (Roser *et al.*, 1996).  $\text{SiO}_2/\text{Al}_2\text{O}_3$  ratios in our sandstone samples range from 4.28 to 9.51, with an overall average of  $6.84 \pm 1.40$ , indicating a low to moderate sediment maturity.

As the degree of weathering is a function chiefly of climate and rates of tectonic uplift (Wronkiewicz and Condie, 1987), increased chemical weathering intensity may reflect the decrease in tectonic activity and/or the change of climate towards warm and humid conditions which are more favorable for chemical weathering in the source region (Jacobson *et al.*, 2003). Therefore, weathering indices of sedimentary rocks can provide useful information of tectonic activity and climatic conditions in the source area. The chemical index most commonly

Table 4. Range of elemental ratios of the Nanpu Sag sandstones in this study compared with the ratios in similar fractions derived from upper continental crust, felsic rocks, mafic rocks, and their probable source rocks

Elemental ratios	Eu/Eu*	(La/Yb) <sub>N</sub>	La/Sc	Th/Sc	Th/Co	Th/Cr
UCC <sup>(a)</sup>	0.65	8.3	2.73	0.97	1.07	0.31
Range of felsic sources <sup>(b)</sup>	0.40–0.94	3.0–27.0	2.5–16.3	0.84–20.5	0.67–19.4	0.13–2.7
Range of mafic sources <sup>(b)</sup>	0.71–0.95	1.1–7.0	0.43–0.86	0.05–0.22	0.04–1.4	0.018–0.046
Archean granite ( <i>n</i> = 5) <sup>1</sup>	0.96–1.77	14.6–94.2	n.g.	n.g.	n.g.	n.g.
	(1.20 ± 0.12)	(38.3 ± 33.6)				
Proterozoic granite ( <i>n</i> = 2) <sup>2</sup>	0.72–0.89	6.7–10.0	n.g.	n.g.	n.g.	n.g.
	(0.83 ± 0.08)	(8.38 ± 2.35)				
Palaeozoic Hercynian granite ( <i>n</i> = 1) <sup>2</sup>	1.23	20.0	n.g.	n.g.	n.g.	n.g.
Mesozoic Yanshanian granite ( <i>n</i> = 24) <sup>3,4,5,6</sup>	0.57–1.20	9.7–30.5	4.99–13.8	0.67–1.49	0.36–11.0	0.13–1.99
	(0.84 ± 0.15)	(18.5 ± 5.6)	(9.61 ± 4.79)	(1.10 ± 0.43)	(2.12 ± 2.96)	(0.84 ± 0.54)
Mesozoic Yanshanian felsic volcanic rock ( <i>n</i> = 44) <sup>3,4,5,6</sup>	0.19–1.01	11.1–26.1	2.03–19.1	0.23–11.91	0.09–2.06	0.03–4.54
	(0.85 ± 0.19)	(17.5 ± 3.71)	(6.02 ± 3.33)	(1.18 ± 2.50)	(0.68 ± 0.46)	(0.93 ± 1.20)
Nm ( <i>n</i> = 5)	0.77–1.08	14.6–17.0	4.11–7.60	0.82–1.86	0.50–0.79	0.08–0.16
	(0.87 ± 0.12)	(16.2 ± 0.9)	(5.02 ± 1.46)	(1.05 ± 0.20)	(0.67 ± 0.12)	(0.11 ± 0.03)
Ngu ( <i>n</i> = 19)	0.57–0.86	7.9–16.2	2.53–6.28	0.68–2.82	0.40–1.69	0.02–0.27
	(0.79 ± 0.07)	(11.8 ± 1.8)	(4.58 ± 0.93)	(1.35 ± 0.47)	(0.81 ± 0.30)	(0.17 ± 0.06)
Ng1 ( <i>n</i> = 9)	0.46–0.83	11.8–14.3	4.24–11.90	0.87–2.97	0.84–1.79	0.10–0.27
	(0.72 ± 0.11)	(13.3 ± 0.9)	(6.83 ± 2.59)	(1.68 ± 0.64)	(1.11 ± 0.32)	(0.18 ± 0.06)
Ed ( <i>n</i> = 4)	0.74–0.87	14.2–17.6	5.87–8.44	1.06–1.51	0.76–0.88	0.15–0.20
	(0.78 ± 0.06)	(15.4 ± 1.5)	(7.15 ± 1.36)	(1.33 ± 0.20)	(0.82 ± 0.05)	(0.17 ± 0.03)

<sup>(a)</sup>Taylor and McLennan (1985).

<sup>(b)</sup>Cullers (1994a, 1994b, 2000), Cullers et al. (1987, 1988). The references represented by numbers 1–5 are shown in Fig. 6. The n.g. represents that the key element is not given in its relevant reference. Values in bracket show mean element ratios and standard deviation.

used to quantify the degree of source area weathering is the Chemical Index of Alteration (CIA; Nesbitt and Young, 1982). The index is defined in molecular proportions as:  $CIA = [Al_2O_3 / (Al_2O_3 + CaO^* + Na_2O + K_2O)] \times 100$ , where CaO\* is the content of CaO incorporated in silicates. This index gives a practical approach to the measurement of feldspar transformation to clay minerals, and the influence of weathering increases with increasing values of CIA. The poor correlations between CIA and other elements, such as CIA–Al<sub>2</sub>O<sub>3</sub> ( $r = -0.17$ ) and CIA–REEs ( $r = -0.37$ ) suggest that grain-size and sorting/clay content are not important factors in determining the CIA ratios. The CIA indices of all analyzed sandstones are in a range of 45.87 to 70.13, with an average of  $57.49 \pm 5.93$ , suggesting that they should have been subjected to low to moderate degrees of chemical alteration. Climatic conditions were warm and semi-humid overall without clear change from the Middle Oligocene to Pliocene (Yao et al., 1994), indicating that it was not a dominating control factor for the variations of CIA value, thus these sandstones would have formed in a relatively intense tectonic environment. From bottom to top, the average values increase from  $46.69 \pm 0.91$  (Ed) to  $62.43 \pm 6.94$  (Ng1), then decrease to  $57.80 \pm 2.75$  (Ngu), to  $56.07 \pm 1.53$  (Nm). This suggests that the intensity or duration of weathering of the sandstones decreased in order of Ng > Nm > Ed Formations. Also the quartz-rich nature of

sandstones from the Ng Formation relative to those from the Nm and Ed Formations is consistent with relatively more intense weathering of the Ng source rocks. In the A–CN–K plot all the sandstones are plotted in a trend from the plagioclase line toward illite indicating the chemical weathering of the source area was chiefly characterized by transformation of plagioclase into clay minerals (illite) (Fig. 8).

For Th/U in sedimentary rocks, weathering and recycling is expected to result in oxidation and removal of U, with a resultant increase in this ratio. Although highly reduced sedimentary environments can have enriched U leading to low Th/U ratios, weathering tends to result in oxidation of insoluble U<sup>4+</sup> to soluble U<sup>6+</sup>, with loss of solution and elevation of Th/U ratios (McLennan and Taylor, 1991). The Th/U ratios of sandstones in the Nanpu Sag range from 2.56 to 7.21, and have an overall mean value of  $4.31 \pm 0.98$ , close to the UCC value of 3.8. In this sense, these sandstones might have been derived from a source subjected to low weathering and recycling.

#### Provenance

REE, Th, Sc, Co, and Cr are quite useful for inferring crustal compositions, because their distribution is not significantly affected by diagenesis and metamorphism and is less affected by heavy-mineral fractionation than that for elements such as Zr and Hf (Bhatia and Crook, 1986;

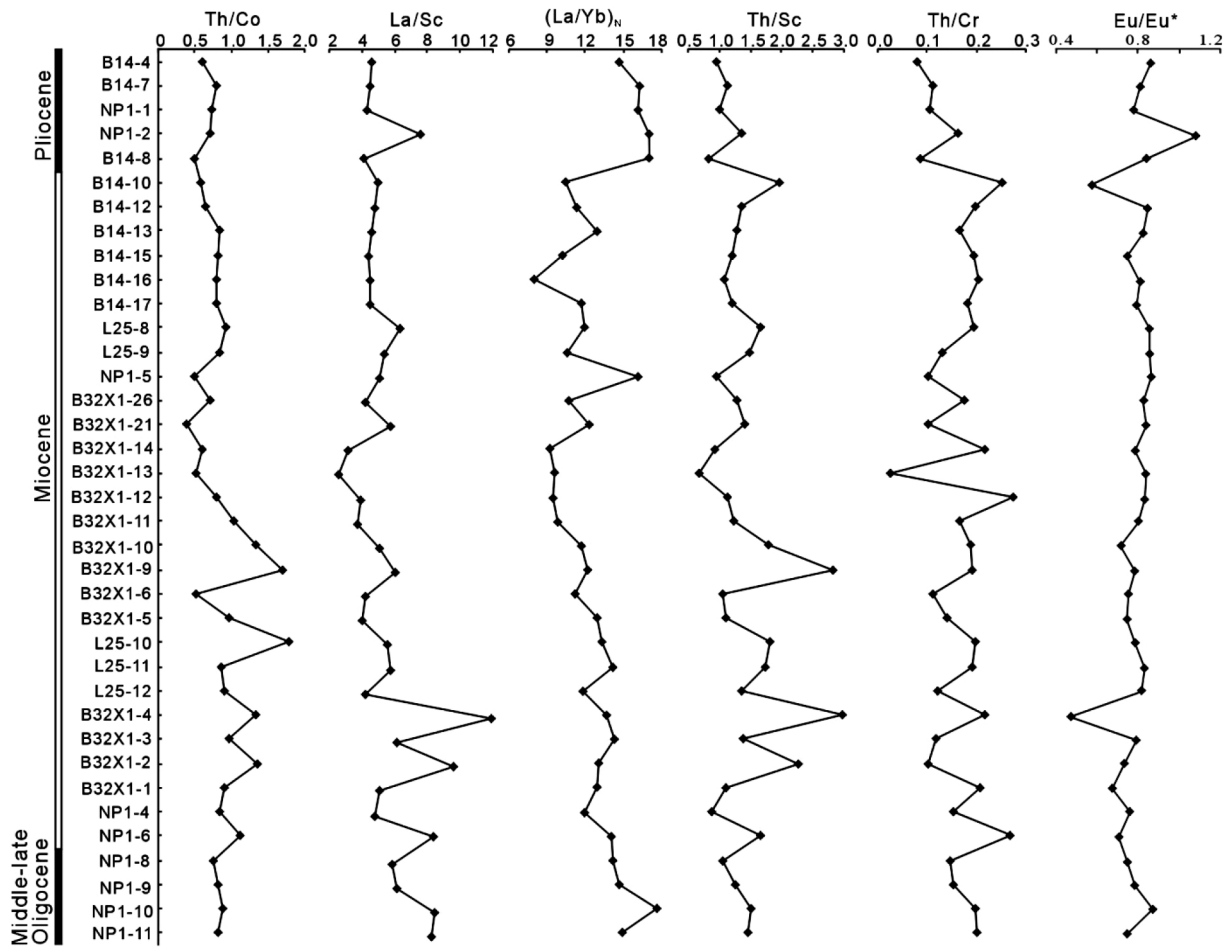


Fig. 9. Stratigraphic variation in  $Th/Co$ ,  $La/Sc$ ,  $(La/Yb)_N$ ,  $Th/Sc$ ,  $Th/Cr$ , and  $Eu/Eu^*$  ratios from the Nanpu Sag. The arrangement orders of the samples represent the sequences of the sedimentary age from Middle Oligocene to Pliocene.

Wronkiewicz and Condie, 1987; McLennan, 2001). Particularly in the absence of sedimentary recycling, ratios such as  $Eu/Eu^*$ ,  $(La/Yb)_N$ ,  $La/Sc$ ,  $Th/Sc$ ,  $Th/Co$ , and  $Th/Cr$  differ significantly in mafic and felsic source rocks and can therefore provide information about the provenance of sedimentary rocks (Cullers *et al.*, 1988; Cullers, 1994a). Even if recycling is important, the ratios may only exhibit modest changes (Wronkiewicz and Condie, 1987). In our study, the  $Eu/Eu^*$ ,  $(La/Yb)_N$ ,  $La/Sc$ ,  $Th/Sc$ ,  $Th/Co$  and  $Th/Cr$  values in the sandstones are more similar to the values for sediments derived from felsic source rocks than those from mafic source rocks, suggesting that these sandstones were probably derived from a felsic terrane (Table 4). In the overall stratigraphic column (Fig. 9), there is no obvious variation trend, except for the Pliocene sandstones.  $Th/Sc$  and  $Th/Cr$  ratios are certainly lower in the Pliocene sandstones, supporting in an increased mafic component, but the contrast for  $La/Sc$  and  $Th/Co$  is not so great.  $Eu/Eu^*$  ratio also increases slightly, which may also reflect mafic detritus or additional

plagioclase. However, the  $(La/Yb)_N$  ratio increases quite sharply; the opposite of what might be expected through an influx of mafic material. Therefore it should be that in the Pliocene sandstones there were influxes of two contrasting materials—mafic material plus highly fractionated and plagioclase-rich granitoid detritus, and this is also supported by the microscopic observation. The sandstones have  $Th/Sc$  ratios between 0.68 and 2.97 (average  $1.38 \pm 0.49$ ) and  $La/Sc$  ratios between 2.53 and 11.94 (average  $5.46 \pm 1.88$ ). These wide ranges suggest that the sediments were not homogenized by sedimentary recycling; that is to say, sandstones of Nanpu Sag do not have the characteristics of mature recycled sediments. Gu *et al.* (2002) used a  $La/Sc$ – $Co/Th$  diagram to identify characteristics of source rocks. In this diagram,  $Co/Th$  ratios range from 0.56 to 2.53 (average  $1.28 \pm 0.42$ ), showing limited variability. Most samples lie close to average Yanshanian felsic volcanic rock ( $n = 44$ ), and a few are near average Yanshanian granite ( $n = 24$ ). All are well away from average basalt and andesite, indicating that

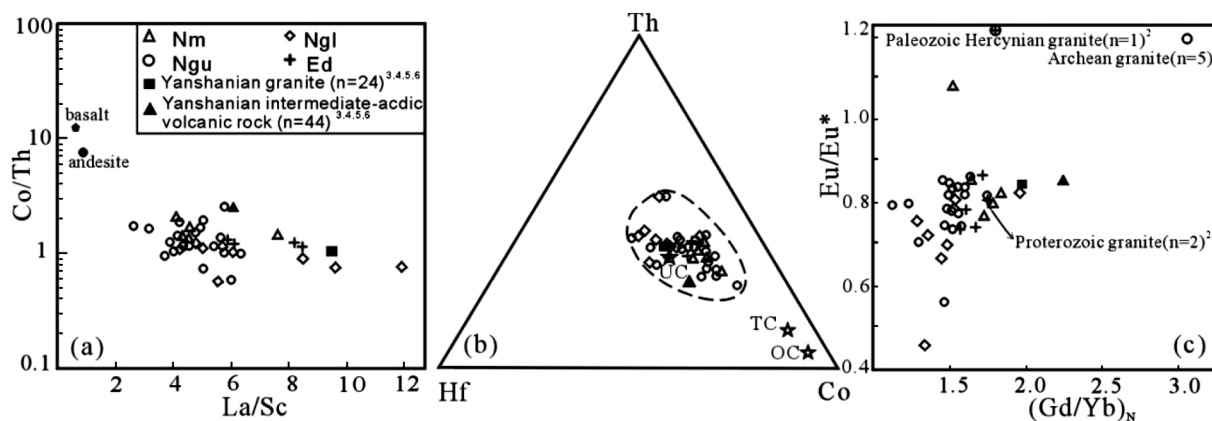


Fig. 10. Provenance discrimination diagrams for the Nanpu Sag sandstones. (a) Co/Th–La/Sc diagram (after Gu *et al.*, 2002). The sandstones fall near the Mesozoic Yanshanian felsic volcanic rock and granite. (b) Th–Hf–Co diagram (Taylor and McLennan, 1985). UC = upper continental crust; TC = total continental crust; OC = average oceanic crust. (c)  $Gd_N/Yb_N$ –Eu/Eu\* (McLennan and Taylor, 1991).  $Gd_N/Yb_N$  ratios of sandstones are between 1.0 and 2.0, and Eu/Eu\* ratios are also low, indicating that they may have been derived from post-Archean upper continental crust. The references represented by numbers 1–5 are shown in Fig. 6. All the samples from the Nanpu Sag are closely related to upper continental crust and Mesozoic Yanshanian granite and intermediate-acid volcanic rock.

the source rocks of these sandstones were mainly felsic (Fig. 10a).

In the Th–Hf–Co diagram (Taylor and McLennan, 1985), all samples plot in the continental crust area and appear to be closely related to UCC. All lie far away from average oceanic crust composition (Fig. 10b). As noted above, all the sandstones have very similar REE patterns, suggesting they have similar source rocks. In comparison with the average upper continental crust (UCC), the samples have low REE abundances but UCC-like patterns. This reinforces the similarity between these sandstone samples and the average upper continental crust. Moreover,  $(Gd/Yb)_N$  ratios of Nanpu Sag sandstones are between 1.13 and 1.96, with an average of  $1.54 \pm 0.16$ . Eu/Eu\* ratio ranges from 0.46 to 1.08 (average  $0.78 \pm 0.09$ ) (Fig. 10c). Both the  $(Gd/Yb)_N$  ratios and the Eu/Eu\* ratios are the characteristic of Post-Archean upper continental crust (McLennan and Taylor, 1991).

Petrological data show that felsic rock fragments predominate in the sandstones (about 80% of total lithics) among various rock fragments. For the whole Bohai Bay Basin, especially its northern Nanpu Sag, the Yanshan Fold Belt was a continuously eroding region and a very important provenance area, along with the evolution of the basin. Previous heavy minerals studies of the Nanpu Sag have shown that the source rocks were mainly from the Yanshan Fold Belt (Li *et al.*, 1998; Mu *et al.*, 2003). Four episodes of intense magmatic activities occurred in the fold belt in pre-Cenozoic time. These produced extensive bodies of intermediate to silicic magmatic rocks, including intermediate-acid volcanic rocks and granite

plutons. In order to constrain the source rocks further, in this study we also collected geochemical data of 76 intermediate-acid magmatic rock from the Yanshan Fold Belt that included 5 Archean granites (Xiao *et al.*, 1994), 2 Proterozoic granites (Tan, 1997), 1 Paleozoic Hercynian granite (Tan, 1997) and 68 intermediate-acid magmatic rocks—consists of 24 granites and 44 felsic volcanic rocks—of the Mesozoic Yanshanian (Xu *et al.*, 1999; Li, W. P., 2003; Wang, Q. *et al.*, 2002; Li, X. Y., 2003). After REE chondrite-normalization, these magmatic rocks show different REE patterns (Fig. 5). The results show that both the REE abundances and REE distribution patterns of the intermediate-acid Yanshanian magmatic rocks are similar to those of the Nanpu Sag sandstone samples. The Archean granites, Proterozoic granites and Paleozoic Hercynian granite not only have lower REE abundances than of the Nanpu Sag sandstones, but also have distinctly different REE patterns. Therefore, we conclude that the source rocks of the sandstones were upper continental crust, and were mainly composed of intermediate-acid magmatic rocks which formed in the Mesozoic Yanshan Fold Belt during the Yanshanian orogeny. This result is consistent with the conclusion reported by Liu *et al.* (2006b) according to REE geochemical characteristics of the Neogene mudstones in the Nanpu Sag.

#### Tectonic setting

Sandstones from different tectonic settings have varying geochemical characteristics (Bhatia, 1983; Roser and Korsch, 1986). Major elements of clastic sedimentary rocks are of value in determining the tectonic settings from

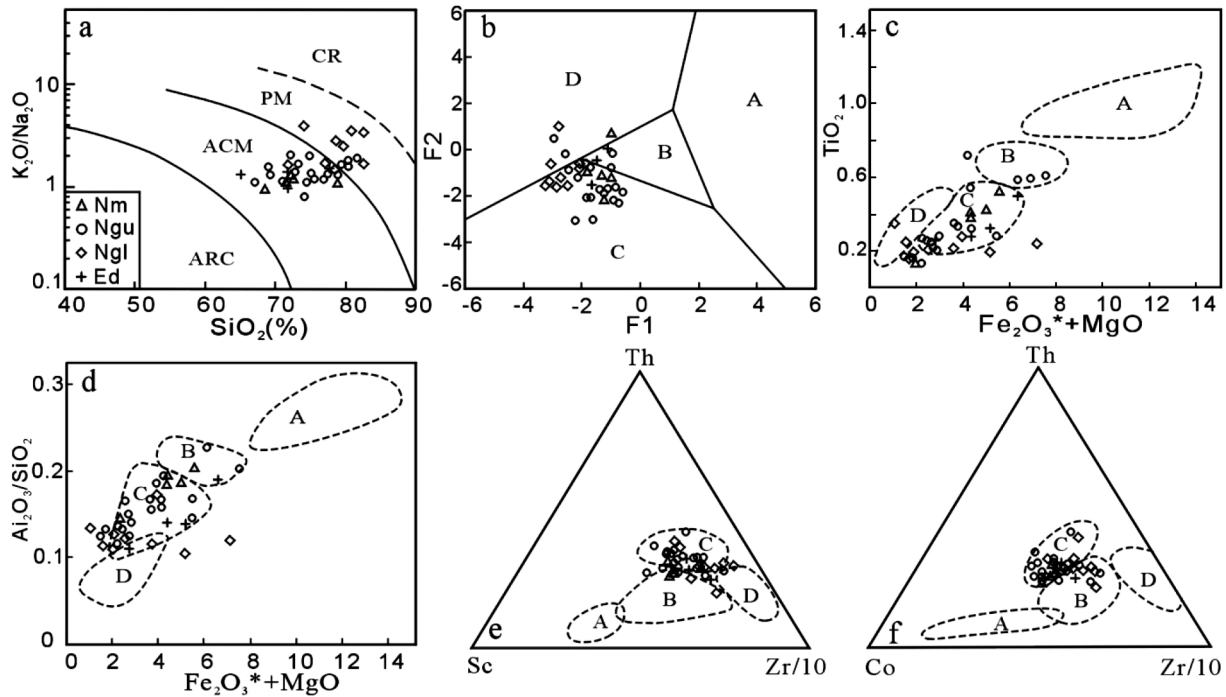


Fig. 11. Tectonic setting discrimination diagrams for the Nanpu Sag sandstones. (a) after Roser and Korsch (1986), modified by Murphy (2000), where A = Oceanic Island Arc (OIA), B = Continental Island Arc (CIA), C = Active continental Margin (ACM), D = Passive continental Margin (PM), CR = continental rift. (b)–(d) after Bhatia (1983). (e) and (f) after Bhatia and Crook (1986). The sandstones mainly plot in the active continental margin field, suggesting an unstable continental setting.

sandstones that have not been strongly affected by weathering and other alteration processes (McLennan *et al.*, 1993). However, some smaller alkali and alkaline earth element cations (e.g.,  $\text{Ca}^{2+}$ ,  $\text{Na}^{+}$  and  $\text{K}^{+}$ ) in terrigenous rocks can be sensitive to weathering conditions in their source area (Wronkiewicz and Condie, 1987). Therefore, it is necessary to determine the degree of alteration of these sandstones. As stated above, the low to moderate CIA values of the sandstones indicate that they were not subjected to severe alteration, and discriminants involving mobile cations can thus be applied. In the  $\text{SiO}_2$ – $\text{K}_2\text{O}/\text{Na}_2\text{O}$  discrimination diagram (Roser and Korsch, 1986; modified after Murphy, 2000), most sandstones fall in the active continental margin field, except for a few in the passive margin field (Fig. 11a). Bhatia (1983) used different major-element contents and their ratios (e.g.,  $\text{Fe}_2\text{O}_3 + \text{MgO}$ ,  $\text{TiO}_2$ , and  $\text{Al}_2\text{O}_3/\text{SiO}_2$ ) as variables to discriminate different tectonic settings. In these diagrams, the Nanpu Sag sandstones mainly plot in active continental margin fields (Figs. 11b, c, d).

Bhatia and Crook (1986) believed Th–Sc–Zr/10 and Th–Co–Zr/10 to be the most useful trace element tectonic discrimination plots. Data from the Nanpu Sag sandstones are relatively scattered (Figs. 11e and f) but most fall within the active continental margin fields, confirming

the conclusion from the major element analysis.

In general, it shows that most Ngl sandstones in Fig. 11 are closer to passive continental margin field than the Ed, Nm, and Ngu sandstones, suggesting that in early Miocene age the structural deformation of the Nanpu Sag is relatively weak, which has been testified by fault activities (Cong and Zhou, 1998). Geochemical characteristics of the sandstones in the Nanpu Sag show that the geotectonic setting was similar to an active continental margin. Although this result can not directly delineate the cause of formation of the Bohai Bay Basin, it suggests a relative unstable intra-continental setting, which is consistent with the general geology of eastern China continent (Yang *et al.*, 1986).

On the basis of geochemical characteristics discussed above, in addition to studies on regional geology (Ye *et al.*, 1985; Allen *et al.*, 1997; Ren *et al.*, 2002), we deduce that the general unstable intra-continental setting controls the multiple-phase rifting activities in the Nanpu Sag and its adjacent areas, which were implied by the stratigraphic variations of geochemical indices in our study. As noted above, the Ed sandstones have relatively low  $\text{SiO}_2$  contents, abundant  $\text{Fe}_2\text{O}_3$  and MgO along with other immobile elements (such as Nb, Th, and REEs), and small CIA and quartz/total feldspar values. These geochemical char-

acteristics suggest that in the Middle–Late Oligocene the Nanpu Sag had intense tectonic activities; this is consistent with the features of the synrift phase (rifting episode II). In this phase, extensional rifting which was probably triggered by subduction roll-back of the oceanic Pacific Plate from the Asian continent were very intense, and the movement of big boundary faults—the Xi'nanzhuang Fault and the Baigezhuang Fault—was a dominative control factor for the subsidence of the Nanpu Sag. Average tectonic subsidence rate from backstripping in this phase was about 160 m/Ma (Wang, H. *et al.*, 2002). The high subsidence rate would result that sediments from the Yanshan Fold Belt were carried and buried so quick that they did not have enough time to endure chemical weathering.

In contrast, the Miocene Ng sandstones have relatively higher contents of SiO<sub>2</sub>, higher values of CIA and quartz/total feldspar, and low contents of Fe<sub>2</sub>O<sub>3</sub> and MgO than those of the Ed sandstones, indicating weak structural deformation in the sag. Before the Miocene Epoch, rifting process had terminated at the end of the Oligocene and was followed by a short period regional uplift and erosion, which was probably resulted from the onset of transpression within eastern Asia, caused by the collision of Australia with the Philippine Sea plate (Allen *et al.*, 1997). Following erosion, the Nanpu Sag as well as other sags in the Bohai Bay Basin were involved in postrift regional subsidence, forming the broad depression (Ren *et al.*, 2002), and regional thermal subsidence was a primary driving force. Only minor and intermittent normal faulting movements existed in this stage, and volcanism was rare except in a small local area near the Xi'nanzhuang Fault. Sedimentary environments changed from alluvial fan, fan delta, shallow-lake facies in the Oligocene to braided-fluvial face in the Miocene. The average tectonic subsidence rate fell to 38 m/Ma (Wang, H. *et al.*, 2002), and this would result that there was more time available for chemical weathering. In the Pliocene Nm sandstones, however, SiO<sub>2</sub> contents, CIA values, and quartz/total feldspar ratios decreased, whereas Fe<sub>2</sub>O<sub>3</sub> and MgO contents increased again. This is also the embodiment of tectonic activity in the Nanpu Sag. In the end of the Pliocene, the Nanpu Sag gradually evolved into structural reactivation period, and rifting movement increased again (Cong and Zhou, 1998). Both activities of faults and regional thermal subsidence controlled the development of this sag. Depositional environment changed from braided-fluvial face to meandering fluvial face. The average tectonic subsidence rate was 123 m/Ma, thus this would result the similar geochemical characteristics with the Ed sandstones. Due to the relatively weak rifting that prevailed, however, the SiO<sub>2</sub> contents and CIA and quartz/total feldspar ratios, and Fe<sub>2</sub>O<sub>3</sub> and MgO contents were higher and lower respectively than those of the Ed sandstones.

## CONCLUSIONS

(1) Geochemical classification—log(SiO<sub>2</sub>/Al<sub>2</sub>O<sub>3</sub>) vs. log(Na<sub>2</sub>O/K<sub>2</sub>O)—shows that the Middle Oligocene–Pliocene sandstones from the Nanpu Sag in the Bohai Bay Basin are mainly arkoses and lithic arenites, plus a few graywackes, in accordance with microscopic observations.

(2) The ratios of quartz/total feldspar, SiO<sub>2</sub>/Al<sub>2</sub>O<sub>3</sub>, Th/U, and CIA ratios show that the sandstone samples have low to moderate degrees of maturity. They were not subjected to intense weathering, suggesting closeness to source area and a low degree of recycling.

(3) Provenance discrimination diagrams (e.g., Qt–F–L, SiO<sub>2</sub>–K<sub>2</sub>O/Na<sub>2</sub>O, Fe<sub>2</sub>O<sub>3</sub> + MgO–Al<sub>2</sub>O<sub>3</sub>/SiO<sub>2</sub>, and Th–Co–Zr/10) and trace-element ratios (Eu/Eu\*, (Gd/Yb)<sub>N</sub>, Th/Co, and La/Sc) show that the source rocks of the sandstones comprised upper continental crust (UCC), and chiefly consisted of felsic magmatic rocks. Comparison of REE distribution patterns between the samples and intermediate-acid magmatic rocks of different age in the Yanshan Fold Belt indicate that the source rocks were mainly in the Mesozoic Yanshanian orogeny.

(4) The Nanpu Sag was in a reactivational intracontinental setting based on coincident results from different tectonic discrimination diagrams, and the intracontinental setting controlled the multiple-phase rifting activities in the Nanpu Sag and its adjacent areas. The geochemical compositional trends of stratigraphy from the Middle Oligocene to Pliocene were material embodiments of the different tectonic activities in the Nanpu Sag.

**Acknowledgments**—This research was financially supported by the Chinese Academy of Sciences Knowledge Innovation Project (No. kzcx2-yw-203-01). Dr. Yehua Shan and Dr. Feng Guo are thanked for their helpful discussions. Three esteemed reviewers (Dr. B. P. Roser, Prof. R. L. Cullers, and an anonymous reviewer) are acknowledged for their constructive suggestions to improve our paper.

## REFERENCES

- Ahmedali, S. T. (1989) X-ray fluorescence analysis in the geological science: Advances in methodology. *Geological Association of Canada, Short Course 7*, 308 pp.
- Allen, M. B., Macdonald, D. I. M., Zhao, X., Vincent, S. J. and Brouet-Menzies, C. (1997) Early Cenozoic two-phase extension and late Cenozoic thermal subsidence and inversion of the Bohai Basin, northern China. *Mar. Pet. Geol.* **14**, 951–972.
- Armstrong-Altrin, J. S., Lee, Y. I., Verma, S. P. and Ramasamy, S. (2004) Geochemistry of sandstones from the Upper Miocene Kudanulam Formation, southern India: Implications for provenance, weathering, and tectonic setting. *J. Sediment. Res.* **74**(2), 285–297.

- Bhatia, M. R. (1983) Plate tectonics and geochemical composition of sandstones. *J. Geol.* **91**, 611–627.
- Bhatia, M. R. and Crook, K. A. W. (1986) Trace element characteristics of graywackes and tectonic setting discrimination of sedimentary basins. *Contrib. Mineral. Petrol.* **92**, 181–193.
- Boynton, W. V. (1984) Cosmochemistry of the rare earth elements: meteorite studies. *Rare Earth Elements Geochemistry* (Henderson, P., ed.), 63–114, Elsevier, Amsterdam.
- Chen, W. P. and Nabelek, J. (1988) Seismic strike-slip faulting and the development of the North China basin. *Tectonics* **7**(5), 975–989.
- Condie, K. C., Philip, D. N. J. and Conway, C. M. (1992) Geochemical and detrital mode evidence for two sources of Early Proterozoic. *Sediment. Geol.* **77**, 51–76.
- Cong, L. Z. and Zhou, H. M., (1998) Polyphase pulls and parts of active rift in Nanpu Sag and their relationship with oil and gas. *Oil & Gas Geology* **19**(4), 296–301 (in Chinese with English abstract).
- Cullers, R. L. (1994a) The controls on the major and trace element variation of shales, siltstones, and sandstones of Pennsylvanian–Permian age from uplifted continental blocks in Colorado to platform sediment in Kansas, USA. *Geochim. Cosmochim. Acta* **58**, 4955–4972.
- Cullers, R. L. (1994b) The chemical signature of source rocks in size fractions of Holocene stream sediment derived from metamorphic rocks in the Wet Mountains region, USA. *Chem. Geol.* **113**, 327–343.
- Cullers, R. L. (2000) The geochemistry of shales, siltstones and sandstones of Pennsylvanian–Permian age, Colorado, USA: Implications for provenance and metamorphic studies. *Lithos* **51**, 181–203.
- Cullers, R. L., Barrett, T., Carlson, R. and Robinson, B. (1987) Rare-earth element and mineralogic changes in Holocene soil and stream sediment: a case study in the Wet Mountains, Colorado, USA. *Chem. Geol.* **63**, 275–297.
- Cullers, R. L., Basu, A. and Suttner, L. J. (1988) Geochemical signature of provenance in sand-size material in soils and stream sediment near the Tobacco Root Batholith, Montana, USA. *Chem. Geol.* **70**, 335–348.
- Dickinson, W. R. and Suczek, C. (1979) Plate tectonics and sandstone composition. *AAPG Bull.* **63**, 2164–2192.
- Dickinson, W. R., Beard, S., Brakenbridge, F., Erjavec, J., Ferguson, R., Inman, K., Knepp, R., Linberg, P. and Ryberg, P. (1983) Provenance of North American Phanerozoic sandstones in relation to tectonic setting. *Geol. Soc. Am. Bull.* **64**, 222–235.
- Feng, R. and Kerrich, R. (1990) Geochemistry of fine-grained clastic sediments in the Archean Abitibi greenstone belt, Canada: implications for provenance and tectonic setting. *Geochim. Cosmochim. Acta* **54**, 1061–1081.
- Fukao, Y. and Maruyama, S. (1994) Geologic implication of the whole mantle P-wave tomography. *J. Geol. Soc. Jpn.* **100**(1), 4–23.
- Gu, X. X., Liu, J. M. and Zheng, M. H. (2002) Provenance and tectonic setting of the proterozoic turbidites in Hunan, south China: geochemical evidence. *J. Sediment. Res.* **72**(3), 393–407.
- Guo, H., Xia, B. and Chen, G. W. (2005) Geochemistry of basalts during Oligocene in Huimin Depression and its geotectonic significance. *Geotectonica et Metallogenia* **29**(3), 303–315 (in Chinese with English abstract).
- Guo, L. Z., Zhu, W. B., Ma, R. S., Sun, Y. and Wang, F. (2003) Discussion on the structural coupling. *Geotectonica et Metallogenia* **27**(3), 197–205 (in Chinese with English abstract).
- Hu, J. Y., Xu, S. B., Tong, X. G. and Wu, H. Y. (1989) The Bohai Bay Basin. *Chinese Sedimentary Basins* (Zhu, X., ed.), 89–105, Elsevier, Amsterdam.
- Ichiki, M., Uyeshima, M., Utada, H., Guoze, Z., Ji, T. and Mingzhi, M. (2001) Upper mantle conductivity structure of the back-arc region beneath Northeastern China. *Geophys. Res. Lett.* **28**(19), 3773–3776.
- Jacobson, A. D., Blum, J. D., Chamberlain, C. P., Craw, D. and Koons, P. O. (2003) Climate and tectonic controls on chemical weathering in the New Zealand Southern Alps. *Geochim. Cosmochim. Acta* **37**, 29–46.
- Jenner, G. J., Longrich, H. P. and Jackson, S. E. (1990) ICP-MS a powerful tool for high precision trace-element analysis in earth sciences: evidence from analysis of selected U. S. G. S. reference samples. *Chem. Geol.* **83**, 133–148.
- Li, W. P. (2003) The geochemistry characteristics and its geodynamics for Mesozoic igneous rocks in Yanshan Orogenic Belt. Dr. Sci. Thesis, Guangzhou Institute of Geochemistry, 27–46 (in Chinese).
- Li, X. Y. (2003) Mesozoic volcanism and constraint on deep geological process in Yanshan Orogenic Belt. Dr. Sci. Thesis, Guangzhou Institute Geochemistry, 34–45 (in Chinese).
- Li, Z., Jiao, Y. Q., Liu, C. H. and Zheng, H. J. (1998) Provenance analysis of heavy minerals in Gaoliu area, Huanghua Depression, Eastern China. *Pet. Explor. Dev.* **25**(6), 5–9 (in Chinese with English abstract).
- Liu, D. Y., Nutman, A. P., Compston, W., Wu, J. S. and Shen, Q. H. (1992) Remnants of  $3800$  Ma crust in the Chinese part of the Sino-Korean craton. *Geology* **20**, 339–342.
- Liu, S. L., Lin, G., Zhou, Y., Gong, F. X. and Zhang, D. S. (2006a) Distribution characteristics of elements in sedimentary rocks of Nanpu Sag and their multiple statistic analysis. *Geology and Resources* **15**(3), 212–217 (in Chinese with English abstract).
- Liu, S. L., Liu, Y. H., Lin, G., Zhou, Y., Gong, F. X. and Zhang, D. S. (2006b) REE geochemical characteristics and geological significance of mudstones from Neogene, Nanpu Sag, Bohai Basin. *Geoscience* **20**(3), 449–456 (in Chinese with English abstract).
- Lu, K. Z., Qi, J. F., Dai, J. S., Yang, Q. and Tong, H. M. (1997) *Tectonic Model of Cenozoic Petroliferous Basin in Bohai Bay Province*. Geological Publishing House, Beijing, 120–208 (in Chinese).
- Ma, X. Y., Liu, H. F. and Wang, W. X. (1983) Mesozoic to Cenozoic rifting and extending in East China. *Acta Geologica Sinica* **57**(1), 22–32 (in Chinese with English abstract).
- McLennan, S. M. (1989) Rare earth elements in sedimentary rocks: influence of provenance and sedimentary processes. *Rev. Mineral. Geochem.* **21**, 169–200.
- McLennan, S. M. (2001) Relationships between the trace element composition of sedimentary rocks and upper conti-

- mental crust. *Geochem. Geophys. Geosyst.* **2**, 86–98.
- McLennan, S. M. and Taylor, S. R. (1991) Sedimentary rocks and crustal evolution: tectonic setting and secular trends. *J. Geol.* **99**, 1–21.
- McLennan, S. M., Hemming, S., McDaniel, D. K. and Hanson, G. N. (1993) Geochemical approaches to sedimentation, provenance and tectonics. *Processes Controlling the Composition of Clastic Sediments* (Johnsson, J. M. and Basu, A., eds.), Special Paper 284, Geological Society of America.
- Mu, L. H., Peng, S. M., Yin, Z. J. and Lei, Y. L. (2003) Sequence stratigraphy and lithofacies palaeogeography of the Shahejie Formation of paleogene in Liuzan Oilfield, Eastern Hebei Province. *Journal of Palaeogeography* **5**(3), 304–315 (in Chinese with English abstract).
- Murphy, J. B. (2000) Tectonic influence on sedimentation along the southern flank of the late Paleozoic Magdalen basin in the Canadian Appalachians: Geochemical and isotopic constraints on the Horton Group in the St. Marys basin, Nova Scotia. *Geol. Soc. Am. Bull.* **112**, 997–1011.
- Nesbitt, H. W. and Young, G. M. (1982) Early Proterozoic climate and plate motions inferred from major element chemistry of lutites. *Nature* **299**, 715–717.
- Nesbitt, H. W. and Young, G. M. (1984) Prediction of some weathering trends of plutonic and volcanic rocks based on thermodynamic and kinetic considerations. *Geochim. Cosmochim. Acta* **48**, 1523–1534.
- Nesbitt, H. W. and Young, G. M. (1996) Petrogenesis of sediments in the absence of chemical weathering: effects of abrasion and sorting on bulk composition and mineralogy. *Sedimentology* **43**, 341–358.
- Nesbitt, H. W., Young, G. M., McLennan, S. M. and Keays, R. R. (1996) Effects of chemical weathering and sorting on the petrogenesis of siliciclastic sediments, with implication for provenance studies. *J. Geol.* **104**, 525–542.
- Pettijohn, F. J., Potter, P. E. and Siever, R. (1973) *Sand and Sandstone*. Springer-Verlag, New York, 618 pp.
- Ren, J. Y., Tamaki, K., Li, S. T. and Zhang, J. X. (2002) Late Mesozoic and Cenozoic rifting and its dynamic setting in Eastern China and adjacent areas. *Tectonophysics* **344**, 175–205.
- Roser, B. P. and Korsch, R. J. (1986) Determination of tectonic setting of sandstone-mudstone suites using SiO<sub>2</sub> content and K<sub>2</sub>O/Na<sub>2</sub>O ratio. *J. Geol.* **94**, 635–650.
- Roser, B. P. and Korsch, R. J. (1988) Provenance signatures of sandstone-mudstone suites determined using discriminant function analysis of major-element data. *Chem. Geol.* **67**, 119–139.
- Roser, B. P., Cooper, R. A., Nathan, S. and Tulloch, A. J. (1996) Reconnaissance sandstone geochemistry, provenance and tectonic setting of the Lower Palaeozoic terranes of the West Coast an Nelson, New Zealand. *New Zeal. J. Geol. Geophys.* **39**, 1–16.
- Tan, G. P. (1997) Geochemical features of granites related with gold deposits in Yanshan Region. *J. Shenyang Inst. Gold Technol.* **16**(1), 23–27 (in Chinese with English abstract).
- Taylor, S. R. and McLennan, S. M. (1985) *The Continental Crust: Its Composition and Evolution*. Blackwell, Oxford, 312 pp.
- Wanas, H. A. and Abdel-Maguid, N. M. (2006) Petrography and geochemistry of the Cambro–Ordovician Wajid Sandstone, southwest Saudi Arabia: Implications for provenance and tectonic setting. *J. Asian Earth Sci.* **26**, 1–14.
- Wang, H., Wang, F. Z., Zhou, H. M. and Dong, Y. X. (2002) *Thermodynamic and Reservoir-forming Dynamic Mechanism of the Evolution Nanpu Sag, Bohai Bay Basin, China*. China University of Geosciences Press, Wuhan, 142–163.
- Wang, Q., Xu, J. F., Zhao, Z. H., Wang, R. J. and Xiong, X. L. (2002) Geochemical characteristics and genesis of Yanshanian intrusive rocks in Fanshan, Hebei province. *Acta Mineral. Sinica* **22**(2), 160–168.
- Wronkiewicz, D. J. and Condie, K. C. (1987) Geochemistry of Archean shales from the Witwatersrand Supergroup, South Africa: source-area weathering and provenance. *Geochim. Cosmochim. Acta* **51**, 2401–2416.
- Xiao, L., Ouyang, Ch. P. and Wang, J. C. (1994) The geology and geochemistry of the Archean granitoids in Qinglong, east Hebei. *J. Guilin Coll. Geol.* **14**(4), 380–386 (in Chinese with English abstract).
- Xu, B. L., Yan, G. H. and Xu, Z. B. (1999) Geochemistry and genetic implication of three series of Yanshanian granite in northern Hebei Province. *Acta Petrologica Sinica* **15**(2), 208–216 (in Chinese with English abstract).
- Xu, Y. G., Chung, S. L., Ma, J. and Shi, L. (2004) Contrasting Cenozoic lithospheric evolution and architecture in western and eastern Sino–Korean Craton: Constraints from geochemistry of basalts and mantle xenoliths. *J. Geol.* **112**(5), 593–605.
- Yang, Z. Y., Cheng, Y. Q. and Wang, H. Z. (1986) *The Geology of China*. Clarendon Press, Oxford, 303 pp.
- Yao, Y. M., Liang, H. J. and Cai, Z. J. (1994) *Tertiary System of China's Oilfields: The Bohai Bay Basin*. Petroleum Industry Press, Beijing, 128–129 (in Chinese).
- Ye, H., Shedlock, K. M., Hellinger, S. J. and Sclater, J. G. (1985) The north China basin: an example of a Cenozoic rifted intraplate basin. *Tectonics* **4**, 153–169.
- Zhang, J. and Shi, Y. L. (2003) Thermodynamics mechanism of the marginal extensional belt of East Asia. *Geotectonica et Metallogenia* **27**(3), 222–227 (in Chinese with English abstract).
- Zhang, K. (1988) Cenozoic extension in Eastern Asia and its geotectonic significance. *Marine Geology & Quaternary Geology* **8**(3), 25–34 (in Chinese with English abstract).
- Zhao, C. Y. (1984) Structural pattern and evolution of the Bohai Gulf, China. *Acta Petrolei Sinica* **5**(1), 1–18 (in Chinese with English abstract).
- Zheng, T. Y., Chen, L., Zhao, L., Xu, W. W. and Zhu, R. X. (2006) Crust-mantle structure difference across the gravity gradient zone in North China Craton: Seismic image of the thinned continental crust. *Phys. Earth Planet. Inter.* **159**, 43–58.